

## THE NUCLEAR X-RAY EMISSION OF NEARBY EARLY-TYPE GALAXIES

S. PELLEGRINI

Astronomy Department, University of Bologna, via Ranzani 1, 40127 Bologna, Italy  
Submitted December 21, 2009; accepted May 11, 2010

### ABSTRACT

Nuclear hard X-ray luminosities ( $L_{X,\text{nuc}}$ ) for a sample of 112 early type galaxies within a distance of 67 Mpc are used to investigate their relationship with the central galactic black hole mass  $M_{\text{BH}}$  (coming from direct dynamical studies or the  $M_{\text{BH}} - \sigma$  relation), the inner galactic structure (using the parameters describing its cuspsiness), the hot gas content and the core radio luminosity. For this sample,  $L_{X,\text{nuc}}$  ranges from  $10^{38}$  to  $10^{42}$  erg s<sup>-1</sup>, and the Eddington ratio  $L_{X,\text{nuc}}/L_{\text{Edd}}$  from  $10^{-9}$  to  $10^{-4}$ , with the largest values belonging to four Seyfert galaxies. Together with a trend for  $L_{X,\text{nuc}}$  to increase on average with the galactic luminosity  $L_{\text{B}}$  and  $M_{\text{BH}}$ , there is a wide variation of  $L_{X,\text{nuc}}$  (and  $L_{X,\text{nuc}}/L_{\text{Edd}}$ ), by up to 4 orders of magnitude, at any fixed  $L_{\text{B}} > 6 \times 10^9 L_{\text{B},\odot}$  or  $M_{\text{BH}} > 10^7 M_{\odot}$ . This large observed range should reflect a large variation of the mass accretion rate  $\dot{M}_{\text{BH}}$ , and possible reasons for this difference are searched for. On the circumnuclear scale, in a scenario where accretion is (quasi) steady,  $\dot{M}_{\text{BH}}$  at fixed  $L_{\text{B}}$  (or  $M_{\text{BH}}$ ) could vary due to differences in the fuel production rate from stellar mass return linked to the inner galactic structure; a trend of  $L_{X,\text{nuc}}$  with cuspsiness is not observed, though, while a tendency for  $L_{X,\text{nuc}}/L_{\text{Edd}}$  to be larger in cuspiers galaxies is present. In fact,  $\dot{M}_{\text{BH}}$  is predicted to vary with cuspsiness by a factor exceeding a few only in hot gas poor galaxies and for large differences in the core radius; for a subsample with these characteristics the expected effect seems to be present in the observed  $L_{X,\text{nuc}}$  values.  $L_{X,\text{nuc}}$  does not show a dependence on the age of the stellar population in the central galactic region, for ages  $> 3$  Gyr; less luminous nuclei, though, are found among the youngest galaxies or galaxies with a younger stellar component. On the global galactic scale,  $L_{X,\text{nuc}}$  shows a trend with the total galactic hot gas cooling rate ( $L_{X,\text{ISM}}$ ): it is detected both in gas poor and gas rich galaxies, and on average increases with  $L_{X,\text{ISM}}$ , but again with a large scatter. The observed lack of a tight relationship between  $L_{X,\text{nuc}}$  and the circumnuclear and total gas content can be explained if accretion is regulated by factors overcoming the importance of fuel availability, as 1) the gas is heated by black hole feedback and  $\dot{M}_{\text{BH}}$  varies due to an activity cycle, and 2) the mass effectively accreted by the black hole can be largely reduced with respect to that entering the circumnuclear region, as in radiatively inefficient accretion with winds/outflows. Finally, differently from  $L_{X,\text{nuc}}$ , the central 5 GHz VLA luminosity shows a clear trend with the inner galactic structure, that is similar to that shown by the total soft X-ray emission; therefore it is suggested that they could both be produced by the hot gas.

*Subject headings:* galaxies: elliptical and lenticular, CD — galaxies: fundamental parameters — galaxies: nuclei — X-rays: galaxies — X-rays: ISM

### 1. INTRODUCTION

In the past years, high angular resolution studies of the centers of early type galaxies have been performed with the *Hubble Space Telescope* (*HST*) in the optical and near infrared, and in the X-rays with *Chandra*, obtaining important results that deeply influenced our understanding of the nature and past evolution of these systems. The first, major *HST* result was that massive black holes (MBHs) are ubiquitous in the centers of spheroids, and linked by tight relationships with the luminosity and central stellar velocity dispersion of their hosts (e.g., Magorrian et al. 1998, Ferrarese & Merritt 2000, Gebhardt et al. 2000), indicative of a strong mutual influence during their formation and evolution. The second *HST* result was that the central brightness profiles of galaxies with  $M_V \lesssim -19$  show either steep brightness cusps or, interior to a break radius  $r_b$ , they flatten markedly in a core with respect to an inner extrapolation of the outer profile. These profiles have been described respectively by a Sérsic or core-Sérsic law (Graham et

al. 2003, Trujillo et al. 2004, Ferrarese et al. 2006, Kormendy et al. 2009) or alternatively by the "Nuker law" (Faber et al. 1997, Lauer et al. 2007a). Cores dominate at the highest luminosities and steep cusps at the lowest, with an intermediate luminosity region of coexistence ( $-20.5 \gtrsim M_V \gtrsim -23$ , Lauer et al. 2007a). The shape of the brightness profile in the inner galactic region has been related to the past formation and evolution of galaxies, with cores created during dry merging events by a black hole binary ejecting stars from the center of the new system (Ebisuzaki et al. 1991, Faber et al. 1997, Milosavljevic et al. 2002, Graham 2004, Gualandris & Merritt 2008), and cusps being preserved or (re)generated during gaseous (wet) mergings. Recently, it was found that coreless elliptical galaxies in the Virgo cluster have extralight at their center, above the inward extrapolation of their outer Sérsic profile (Kormendy et al. 2009), the result of a wet merger induced starburst (see also Hopkins et al. 2009a) or of AGN induced starburst activity (Ciotti & Ostriker 2007). Moreover, the presence of steep cusps or cores correlates with other fundamental galactic

properties, even more tightly than how these properties correlate with the galactic luminosity: core galaxies generally have boxy isophotes, are slow rotators and triaxial systems, while cusp galaxies are disk, fast rotators and axisymmetric (Kormendy & Bender 1996, Faber et al. 1997); core galaxies show a large range of radio and X-ray luminosities, while cusp galaxies are confined below a threshold (Bender et al. 1989; Pellegrini 1999, 2005a; Capetti & Balmaverde 2005; Pasquali et al. 2007). Pellegrini (2005a) also attempted an investigation of the relation between the X-ray nuclear emission ( $L_{X,nuc}$ ) and the inner core/cusp profile, but the study was limited by the small number of nuclei with known  $L_{X,nuc}$  available.

Launched in 1999, the *Chandra* satellite has now pointed a large number of early type galaxies, with an unprecedented angular resolution in the X-rays of less than  $1''$ . For the first time measurements of the nuclear X-ray emission down to values as low as  $10^{39}$  erg  $s^{-1}$  and out to distances of  $\sim 60$  Mpc have been obtained. The MBHs of the local universe turned out to be typically radiatively quiescent and very sub-Eddington emitters (Loewenstein et al. 2001, Soria et al. 2006a, Zhang et al. 2009, Gallo et al. 2008, 2010). In a number of cases the mass accretion rate on the MBH could be estimated (e.g., Di Matteo et al. 2003, Pellegrini 2005b) and the radiative quiescence was interpreted in terms of radiatively inefficient accretion (Narayan & Yi 1995), possibly with the mechanical power dominating the total output of accretion (e.g., Allen et al. 2006). However, many aspects of accretion in the local universe remain unknown: what determines  $L_{X,nuc}$ ? Is there any relation of  $L_{X,nuc}$  or its Eddington-scaled value with the galactic luminosity or the mass of the central supermassive black hole  $M_{BH}$ ? or with the inner stellar profile, that has been linked to the past galactic evolution and other major global galactic properties? or with the hot gas content? Answering these questions is important for a complete understanding of the MBH-host galaxy coevolution process.

In this work we have collected all early type galaxies (E and S0) out to a distance of  $\sim 67$  Mpc with known  $L_{X,nuc}$ , based mostly on data coming from *Chandra* pointings; a total of 112 galaxies resulted with  $L_{X,nuc}$  measured or with an upper limit on it. The sample includes also most of the early type galaxies with a direct measurement of  $M_{BH}$  via dynamical studies currently available; for the other galaxies, the central stellar velocity dispersion allows for an estimate of  $M_{BH}$  via the  $M_{BH} - \sigma$  relation. For 81 of these 112 galaxies the central stellar profile shape has been measured with *HST*. The sample is described in Sect. 2, the observational evidences about relationships between  $L_{X,nuc}$ ,  $M_{BH}$ , the central stellar structure and the radio luminosity are presented in Sect. 3, the results are discussed in Sect. 4 (that examines also the relationship between  $L_{X,nuc}$  and the galactic hot gas luminosity); the conclusions are summarized in Sect. 5.

## 2. THE SAMPLE

The morphological type of the sample includes E and S0 objects, that is early type galaxies with numerical code  $t \leq -2$  according to the revised de Vaucouleurs morphological type defined in RC2. A distance limit of  $\sim 70$  Mpc was set to allow for the possibility of a measurement of  $L_{X,nuc}$  (or an upper limit on it) with *Chandra* down to

$\sim 10^{39}$  erg  $s^{-1}$  even for the most distant objects, and of a measurement of the inner light profile from *HST* data for a large fraction of the objects (most cores have a radius  $< 500$  pc). A selection of galaxies with the chosen morphological properties and distance limit was performed with the Hyperleda catalog<sup>1</sup>. The resulting list was then cross-correlated with the list of *Chandra* pointings, using the Web ChaSeR (Chandra Archive Search and Retrieval Interface<sup>2</sup>), to find the objects with X-ray information on their nuclei. Published works as of December 2009 based on these pointings provide a detection or upper limit for the nuclear luminosity  $L_{X,nuc}$  for 97 galaxies. In order to avoid possible contamination from soft hot gaseous emission,  $L_{X,nuc}$  was taken in the 2–10 keV band, or converted to it based on the spectral shape used to derive it. The object list, with adopted distances,  $L_{X,nuc}$  values and references for them, is given in Tab. 1.

For the objects in this list, the light profile shape in the inner regions was then searched. Two central slopes have been considered previously (Lauer et al. 1995, Rest et al. 2001, Lauer et al. 2007a):  $\gamma'$ , the local slope evaluated at the *HST* angular resolution limit, and  $\gamma$ , the slope describing the brightness profile  $I(R) \propto R^{-\gamma}$  interior to a break radius  $r_b$ , when adopting a “Nuker law” profile description (a broken power law with a smooth transition from the outer slope to the inner slope  $\gamma$ ). Steep inner cusps have  $\gamma$  and  $\gamma'$  larger than 0.5, and their host galaxies are called “power law” or “cusp” galaxies; cores have  $\gamma$  and  $\gamma'$  smaller than 0.3 (with  $\sim 10\%$  of galaxies with  $\gamma < 0.3$  that have  $\gamma' > 0.3$ ); “intermediate” systems are a minority and have  $\gamma$  or  $\gamma'$  between 0.3 and 0.5. In core galaxies a well defined break radius  $r_b$  marks a rapid transition from the outer profile to a much shallower inner slope; cusp galaxies retain a steep slope into the resolution limit. The definition of what constitutes a core (i.e., a break with respect to a Sérsic function fitted to the outer profile, or an inner slope  $\gamma < 0.3$  in the Nuker function fit) is different for the two descriptions using the two functions, but gives the same classification as core or cusp galaxy for most galaxies (Kormendy et al. 2009). For most of the galaxies in table 1, the inner profile shape comes from the large compilation of Lauer et al. (2007a), who combined the results of previous *HST* investigations of the central structure of early-type galaxies, after transformation to a common band and distance scale; for other 18 galaxies the Nuker law description of the *HST* profile is taken from Capetti & Balmaverde (2005; these are marked in col. 5 in Tab. 1). For the purpose of investigating the relationship between  $L_{X,nuc}$  and the inner galactic structure with as many objects as possible, the initial sample of 97 galaxies was enlarged with 15 objects with inner *HST* slope measured. Of these, 7 follow all the adopted selection criteria, but their  $L_{X,nuc}$  comes from *ROSAT* HRI pointings (with an angular resolution of  $\sim 5''$ , from Liu & Bregman 2005); the other 8 galaxies, with  $L_{X,nuc}$  from *Chandra* data, have a type later than  $t=-2$ , though still within the S0 range<sup>3</sup>. Tab. 1 then includes 112 galaxies, 47 of core type, 7 intermediate, and

<sup>1</sup> <http://leda.univ-lyon1.fr>

<sup>2</sup> <http://asc.harvard.edu/cda/chaser.html>

<sup>3</sup> These 8 galaxies are NGC7743 ( $t=-0.9$ ), NGC524, NGC3945 ( $t=-1.2$ ), NGC4382, NGC5866 ( $t=-1.3$ ), NGC4459, NGC4111 ( $t=-1.4$ ), NGC1316 ( $t=-1.7$ ). For reference, type S0a has  $t=0$ .

27 of cusp type. The profile classification (cusp or core) is based on the value of  $\gamma$ , given in tab. 1; this classification is always coincident with that given by  $\gamma'$ , except for 7 cases that become "cuspiers" when considering  $\gamma'$  instead of  $\gamma^4$ . The results of this work are unchanged when using  $\gamma'$  instead of  $\gamma$ . Other quantities used in the following and not given in Tab. 1 are the break radii  $r_b$  and effective radii  $R_e$ ; these are taken from Lauer et al. (2007a) and Capetti & Balmaverde (2005);  $r_b$  ranges from a few parsecs to few hundreds of parsecs.

Finally, Tab. 1 lists the masses of the central MBHs, taken from specific measurements for a number of galaxies, and from the  $M_{BH} - \sigma$  relation for the other cases, as specified in the table. The adopted  $M_{BH} - \sigma$  relation is that recently derived for ellipticals (Gültekin et al. 2009), in which the central stellar velocity dispersion  $\sigma$  from the Hyperleda catalog is inserted; this relation has an intrinsic scatter of 0.31 dex in  $\log M_{BH}$ . Note that  $M_{BH}$  values estimated from the  $M_{BH} - L_V$  relation of early type galaxies (where  $L_V$  is the V-band luminosity; Gültekin et al. 2009) can be larger than those derived from the  $M_{BH} - \sigma$  relation, for  $M_{BH} \lesssim 10^7 M_\odot$  [see also Gallo et al. (2008)].

The galaxies in Tab. 1 reside in all types of environment, going from being isolated to being at the center of a cluster (as NGC4486 in Virgo) or a group. They also span a large range of activity, from being classified as an optical or radio AGN (e.g., Seyfert or FRI) to inactive. Their optical nuclear spectra have been classified as absorption nuclei (i.e., without emission lines) or, when emission lines are present, mostly as LINERs, with a minority of Seyfert and transition nuclei (intermediate between HII and LINERs; Ho et al. 1997).

### 3. OBSERVATIONAL RESULTS

Figure 1 shows the relationship between  $L_{X,nuc}$  and the B-band galactic luminosity  $L_B$ . Considering the whole  $L_B$  range,  $L_{X,nuc}$  increases on average with  $L_B$ . However, in the well populated region of the plot, for  $L_B > 6 \times 10^9 L_{B\odot}$ ,  $L_{X,nuc}$  does not present a clear trend with  $L_B$  but shows instead a very large scatter of  $\sim 4$  orders of magnitude, going from the lowest detectable  $L_{X,nuc}$  values in the nearest galaxies ( $\sim 10^{38}$  erg s $^{-1}$ ) to the highest  $L_{X,nuc}$  values ( $\gtrsim 10^{42}$  erg s $^{-1}$ ) that belong to Seyfert nuclei (NGC2110, NGC3516, NGC5128, NGC5283; all these are S0 galaxies, consistent with the observation that Seyfert nuclei reside mostly in spirals and S0s, e.g., Malkan et al. 1998). Similar considerations hold for fig. 2, where  $L_B$  is replaced by  $M_{BH}$ , as expected given the Magorrian relation between the spheroid luminosity and the MBH mass (Magorrian et al. 1998): there is an overall trend for  $L_{X,nuc}$  to increase with  $M_{BH}$ , but in the well populated region, for  $M_{BH} > 2 \times 10^7 M_\odot$ ,  $L_{X,nuc}$  shows a very large scatter, of  $\sim 4$  orders of magnitude. Figures 1 and 2 show cusp and core galaxies be-

ing more frequent respectively at the lowest and highest  $L_B$  (and  $M_{BH}$ ) values, but with a large intermediate region of overlap; more importantly, these figures also show that both types cover the whole large range of  $L_{X,nuc}$ .

Figure 3 shows the relation between  $L_{X,nuc}$  scaled by the Eddington luminosity [i.e.,  $L_{X,nuc}/L_{Edd}$ , where  $L_{Edd} = 1.25 \times 10^{38} M_{BH} (M_\odot)$  erg s $^{-1}$ ] and  $M_{BH}$ . Since  $L_{Edd}$  is proportional to  $M_{BH}$ , the lower envelope of the  $L_{X,nuc}$  values in fig. 2 (a straight horizontal line at  $L_{X,nuc} \sim 10^{38}$  erg s $^{-1}$ ) translates in a lower envelope of  $L_{X,nuc}/L_{Edd}$  values that is a line with slope -1, shown in fig. 3 as a dotted line. Above this line, a large scatter of  $\sim 3 - 4$  orders of magnitude in  $L_{X,nuc}/L_{Edd}$  is evident also in this plot. Again, both core and cusp galaxies cover a large range of  $L_{X,nuc}/L_{Edd}$ ; in this case, though, the "cuspiers" types seem to reach highest Eddington ratios of  $10^{-4} - 10^{-3}$  and the core types to be confined below  $L_{X,nuc}/L_{Edd} < 10^{-4.5}$ . Except for few very nearby galaxies, Eddington ratios similarly low cannot be reached at the lowest and at the highest  $M_{BH}$  values, due to the limit marked by the dotted line; but the highest Eddington ratios, for which there are no limits, tend to correspond to the lower  $M_{BH}$ . A similar result was obtained for nearby late type galaxies (Zhang et al. 2009) and for the 100 spheroidal galaxies of the ACS Virgo cluster survey studied by Gallo et al. (2010). In the latter survey,  $L_{X,nuc}$  was estimated with *Chandra* down to a limit of  $L(0.5-7 \text{ keV}) = 3.7 \times 10^{38}$  erg s $^{-1}$  for a sample with stellar masses peaking below  $10^{10} M_\odot$  and MBH masses below  $10^8 M_\odot$ ; the Eddington ratio was found to decrease on average as  $M_{BH}^{-0.62}$ , with a scatter of 0.46 dex. This trend is consistent with the distribution of the  $L_{X,nuc}$  values in fig. 3, though the large scatter here dominates. The average decrease of the Eddington ratio with increasing  $M_{BH}$  was interpreted as a manifestation of down-sizing in black hole accretion (Gallo et al. 2010, Schawinski et al. 2010).

In order to better evidence any possible relationship between  $L_{X,nuc}$  and the inner light profile,  $L_{X,nuc}$  and  $L_{X,nuc}/L_{Edd}$  were plotted against the slope of the central light profile  $\gamma$  (fig. 4). As already suggested by figs. 1 and 2, fig. 4 shows that  $L_{X,nuc}$  spans the whole large range of values, from  $\sim 10^{38}$  to  $\gtrsim 10^{42}$  erg s $^{-1}$ , at all  $\gamma$ 's. A similar result holds for  $L_{X,nuc}/L_{Edd}$  (fig. 4, lower panel), though here the highest  $L_{X,nuc}/L_{Edd}$  values among core galaxies remain lower than those of intermediate and cusp galaxies, as seen from fig. 3. This possible increase of the upper envelope of values of  $L_{X,nuc}/L_{Edd}$  with  $\gamma$ , though requiring a larger and complete sample for a firm conclusion, may be real, given that the galaxies considered here already include more core than cusp cases, and that such an increase is expected to arise, when considering the trend for the Eddington ratio to increase for  $M_{BH}$  decreasing (fig. 3), and the trend for  $M_{BH}$  to decrease on average with  $\gamma$  increasing (as shown in fig. 5 for the present sample). This latter behavior is a consequence of the Magorrian  $M_{BH} - L_B$  relation coupled with the weak  $\gamma - L_B$  anti-correlation (Faber et al. 1997 and Sect. 1). Another possible reason for an increase of  $L_{X,nuc}/L_{Edd}$  with  $\gamma$  is discussed in Sect. 4.1.

Finally, to explore further a possible link with the inner galactic structure, we also considered the relation of  $L_{X,nuc}$  with the break radius  $r_b$ , and with  $r_b$  rescaled

<sup>4</sup> These are 5 cores and one intermediate that become cusps, and one core that becomes intermediate; all these cases are marked in the following figures with a special symbol, as explained in the captions. Note that all galaxies with  $\gamma$  in Tab. 1 have  $M_V < -19$  (from the apparent magnitudes in Hyperleda, and for the distances adopted in Tab. 1), a luminosity range where low  $\gamma < 0.3$  values are associated only to cores in massive ellipticals, and high  $\gamma$ 's unequivocally identify coreless galaxies (Trujillo et al. 2004, Lauer et al. 2007a).

by  $R_e$ . Only core galaxies were considered, for which  $r_b$  is a representative scale for the radial extent of the core (Lauer et al. 2007b). When plotted against  $r_b$ ,  $L_{X,\text{nuc}}$  covers the same large range of values differing by  $\sim 3$  orders of magnitude already seen in the previous figures, and shows no trend with  $r_b$  or  $r_b/R_e$ . The same holds for  $L_{X,\text{nuc}}/L_{\text{Edd}}$ .

### 3.1. The different relation with cuspieness of $L_{X,\text{nuc}}$ and the radio luminosity

As mentioned in Sect. 1, for a sample of galaxies with central light profiles measured from *HST* data, and with 5 GHz radio fluxes estimated from a VLA survey with a  $\sim 3 - 5''$  FWHM resolution, Capetti & Balmaverde (2005) found the radio emission of core galaxies to cover a large range of values, differing by orders of magnitude, while that of cusp galaxies to be confined below  $L_R \sim 3 \times 10^{21}$  W Hz $^{-1}$ . The origin of this threshold in radio luminosity for cusp galaxies remained ambiguous, because galaxies with a higher intrinsic optical luminosity have a higher probability to be strong radio emitters, with respect to less luminous galaxies (e.g., Mauch & Sadler 2007). This is true also for the Capetti & Balmaverde (2005) sample, whose  $L_R - M_K$  relation (where  $M_K$  is the K-band absolute magnitude) shows no radio source with  $L_R$  above the threshold of  $3 \times 10^{21}$  W Hz $^{-1}$  associated to a host with  $M_K > -24$ . Since there are only few cusp galaxies in their sample with  $M_K < -24$ , it cannot be concluded whether the threshold is related to a different nuclear structure, or to cusp galaxies populating scarcely the  $M_K$  range where the brightest radio sources are found.

Both the radio and the X-ray emission are signatures of MBH accretion, but fig. 4 (upper panel) shows clearly the lack of a threshold for  $L_{X,\text{nuc}}$  similar to that found for  $L_R$ ; therefore, the behavior of  $L_{X,\text{nuc}}$  and  $L_R$  with respect to the presence of a core in the stellar light profile is here revisited. Figure 4 was then remade just for the Capetti & Balmaverde (2005) sample, that includes 51 objects, 42 of which are in Tab. 1; all these 42 galaxies have  $M_B < -18.6$ , a luminosity range where low  $\gamma < 0.3$  values are associated only to cores in massive ellipticals (Trujillo et al. 2004). For this sample, figure 6 shows the relationship between  $\gamma$  and the 5 GHz core luminosity  $L_{R,\text{core}}$  from the VLA survey (taken from Capetti & Balmaverde 2006 or Balmaverde & Capetti 2006, and rescaled for the distances in tab. 1). The figure shows again a different behavior with respect to  $\gamma$  of  $L_{X,\text{nuc}}$  and of  $L_{R,\text{core}}$ : while there is an L-shape distribution of  $L_{R,\text{core}}$  with respect to the inner light profile, with galaxies of all types below  $L_{R,\text{core}} \sim 10^{38}$  erg s $^{-1}$  and only core galaxies above,  $L_{X,\text{nuc}}$  shows the same lack of a threshold found in fig. 4. We note that the VLA radio data used to derive the luminosities in fig. 6 do not separate well the core emission from any extended structure, and they tend to overestimate the core flux when there is extended radio emission (Balmaverde & Capetti 2006). These findings are discussed in Sect. 4.4.

## 4. DISCUSSION

Hard X-ray emission is a major signature of accretion on a MBH, both in the standard disk plus hot corona modality (Haardt & Maraschi 1993) and in the radiatively inefficient modality (RIAF, Narayan & Yi 1995)

that is expected to establish at the low Eddington ratios of the sample investigated here (fig. 3). In fact, the nuclei in this sample are highly sub-Eddington for any bolometric correction  $L_{\text{bol}}/L_{X,\text{nuc}}$  that can be plausibly adopted: from  $\sim 10$  for low luminosity AGNs, as indicated by observations (e.g., Ho 2008) and by the RIAF modeling (Mahadevan 1997), up to 40–70 for standard, bright AGNs (Vasudevan & Fabian 2007). For radiatively inefficient accretion  $L_{X,\text{nuc}}$  should scale inversely proportional to  $M_{\text{BH}}$ , at fixed mass accretion rate on the MBH,  $\dot{M}_{\text{BH}}$  (Mahadevan 1997; see also K rding et al. 2006). What instead dominates in fig. 1 is a wide variation of  $L_{X,\text{nuc}}$  by 3–4 orders of magnitude at any fixed  $M_{\text{BH}} > 10^7 M_{\odot}$ . A large variation of  $L_{X,\text{nuc}}$  of a similar extent was obtained also for other local samples, made of galaxies of types later than that discussed here and residing within 15 Mpc (Zhang et al. 2009), or for the nuclei in the Palomar survey (Ho 2009).

Intrinsic variability of  $L_{X,\text{nuc}}$  cannot account entirely for the large spread in figs. 1–3, since amplitude variations of low luminosity AGNs are typically small (Ptak et al. 1998) and the largest keep within a factor of a few (Pian et al. 2009). The large range of  $L_{X,\text{nuc}}$  and of  $L_{X,\text{nuc}}/L_{\text{Edd}}$  means then that physical quantities other than the size of  $M_{\text{BH}}$  play an important role. In the RIAF models a number of parameters describe the complex physics of accretion (e.g., the ratio of gas to magnetic pressure, the viscosity, the turbulent energy that heats the electrons), but their variation is not expected to account for  $L_{X,\text{nuc}}$  differences as large as those in figs. 1–3 (e.g., Di Matteo et al. 2003). Another major parameter determining  $L_{X,\text{nuc}}$  is the mass accretion rate on the MBH,  $\dot{M}_{\text{BH}}$ ; for example, at fixed  $M_{\text{BH}}$ ,  $L_{X,\text{nuc}}$  scales as  $\dot{M}_{\text{BH}}^2$  for radiatively inefficient flows (Narayan & Yi 1995). Below we discuss possible variations of  $\dot{M}_{\text{BH}}$  produced by the inner galactic structure, that determines how much mass is shed by stars in the circumnuclear region and then the fuel available for the MBH. In fact, the present sample is defined morphologically to include galaxies with a typically old stellar population, and in these systems the black hole growth is regulated by the rate at which evolved stars lose their mass, as shown for a large sample of nearby galaxies drawn from the Sloan Digital Sky Survey (Kauffmann & Heckman 2009). In the following Section 4.1 we assume that accretion is a (quasi) steady process; then in Section 4.3 we consider the possibility that accretion is unsteady.

### 4.1. The mass accretion rate, the inner galactic structure and the total gas content

Numerical simulations of the collective evolution of stellar mass losses (Parriott & Bregman 2008), for stellar mass distributions as steep as revealed by *HST* in the central galactic region, showed that they establish an inflow towards the MBH (Pellegrini & Ciotti 1998, Pellegrini et al. 2007a). The size of the inflowing region  $r_{\text{in}}$  can range from being of the order of the MBH accretion radius  $r_a$  ( $r_a \propto M_{\text{BH}}/T_{\text{ISM}} = 10 - 100$  pc for typical values of the ISM temperature  $T_{\text{ISM}}$  and  $M_{\text{BH}} = 10^8 - 10^9 M_{\odot}$ , e.g., Soria et al. 2006a) to few kpc. The stellar mass losses within  $r_{\text{in}}$  then make up the fuel to which  $\dot{M}_{\text{BH}}$  should be proportional. Since the rate at which a given volume of a galaxy is replen-

ished by mass losses from stars during their passive evolution is just proportional to the local stellar luminosity (e.g., Ciotti et al. 1991, David et al. 1991),  $\dot{M}_{\text{BH}}$  and then  $L_{\text{X,nuc}}$  should depend on the shape of the stellar density within  $r_{\text{in}}$ . On average, core galaxies have a lower central surface brightness and central stellar density than cusp ones (Faber et al. 1997, Gebhardt et al. 1996, 2003, Kormendy et al. 2009), and core galaxies with larger cores have a lower central density than those with smaller cores. This determines that, at similar  $L_{\text{B}}$  (or equivalently  $M_{\text{BH}}$ ), cusp galaxies produce locally more fuel for accretion than core ones, and galaxies with smaller  $r_b$  produce more fuel than those with larger  $r_b$ , which should correspond to a higher  $L_{\text{X,nuc}}$  and  $L_{\text{X,nuc}}/L_{\text{Edd}}$ <sup>5</sup>. To quantify this difference, we can calculate for example how the stellar mass within three fiducial radii of  $r_{\text{in}} = 10, 100$  and  $10^3$  pc, representative of  $r_a$  and of larger inflowing regions, varies between a pure Sérsic profile and a core-Sérsic one that is identical to the pure Sérsic except for an inner slope  $\gamma = 0.1$  within a break radius  $r_b$  (e.g., Graham et al. 2003). We choose two effective radii ( $R_e = 8$  or  $12$  kpc) and Sérsic indices ( $n = 6$  or  $n = 8$ ) appropriate for core galaxies of  $L_{\text{B}} = 2$  or  $5 \times 10^{10} L_{\text{B},\odot}$  (Ferrarese et al. 2006, Kormendy et al. 2009). Within  $r_{\text{in}} = 10$  pc, a pure Sérsic profile has a mass 2–3 times larger than with  $r_b = 10$  pc, and  $\sim 25$  ( $n = 6$ ) or  $\sim 50$  ( $n = 8$ ) times larger than with  $r_b = 100$  pc. Within  $r_{\text{in}} = 100$  pc, a pure Sérsic has  $\sim 3$  times more mass than a core-Sérsic with  $r_b = 100$  pc, and  $\sim 10$  ( $n = 6$ ) or  $\sim 20$  ( $n = 8$ ) times more than for  $r_b = 300$  pc. Within  $r_{\text{in}} = 1$  kpc, instead, a pure Sérsic has a mass only  $\lesssim 20\%$  larger than with  $r_b = 100$  or  $300$  pc, both for  $n = 6$  and  $n = 8$ . Therefore the difference in fuel production can be significant (i.e., larger than a factor of a few) only for small inflow regions of the order of  $r_{\text{in}} \gtrsim r_a$ , and large break radii  $r_b > 10$  pc, while it vanishes for  $r_{\text{in}} \gtrsim 1$  kpc<sup>6</sup>. Small  $r_{\text{in}}$  correspond to low galactic hot gas contents, as found at  $L_{\text{B}} \lesssim 3 \times 10^{10} L_{\text{B},\odot}$  (David et al. 2006), and whenever the total galactic soft X-ray emission  $L_{\text{X,tot}}$  rescaled by  $L_{\text{B}}$  (that is  $L_{\text{X,tot}}/L_{\text{B}}$ ) is low (Pellegrini & Ciotti 1998); a difference in  $L_{\text{X,nuc}}$  could then best manifest itself for these objects. Similar numbers to those obtained above for the stellar mass variation within  $r_{\text{in}}$  were obtained in the calculation of the stellar mass fraction within different radii for the Lauer et al. (2007a) sample, divided in bins of fixed total stellar mass; this fraction was found to show a scatter of  $\sim 1$  order of magnitude within  $0.001 R_e$  (Hopkins et al. 2009b). To summarize, 1) a difference in the inner galactic structure can produce a different amount of circumnuclear material at fixed  $L_{\text{B}}$  (or  $M_{\text{BH}}$ ), and may then contribute to the scatter in figs. 1–3, though it cannot account for the

bulk of it, since for most galaxies the variation in gas production within  $r_{\text{in}}$  will not exceed a factor of a few; 2) possible differences in  $\dot{M}_{\text{BH}}$  are expected to exceed a factor of 2–3 only at the lowest  $L_{\text{X,tot}}/L_{\text{B}}$ , and should then be searched for in such galaxies.

To pursue further point 2) above, we extracted from the list of galaxies in tab. 1 a sample of core galaxies with low  $L_{\text{X,tot}}/L_{\text{B}}$ . The total X-ray luminosity  $L_{\text{X,tot}}$  was taken from O’Sullivan et al. (2001), based on *ROSAT* observations for a thermal spectrum of  $kT = 1$  keV, and then most sensitive to the soft gaseous emission; we considered the ratio  $L_{\text{X,tot}}/L_{\text{B}}$  to correspond to a low hot gas content when  $L_{\text{X,tot}}(\text{erg s}^{-1})/L_{\text{B}}(L_{\text{B},\odot}) \lesssim 30.21$ , that is below the upper limit on the expected contribution from X-ray binaries (from Kim & Fabbiano 2004). Figure 7 shows  $L_{\text{X,nuc}}$  and  $L_{\text{X,nuc}}/L_{\text{Edd}}$  versus  $r_b$  and  $r_b/R_e$  for this subsample: a trend in the predicted direction is present for the upper envelope of the  $L_{\text{X,nuc}}$  and  $L_{\text{X,nuc}}/L_{\text{Edd}}$  values, that decreases for increasing  $r_b$ .

#### 4.2. $L_{\text{X,nuc}}$ and the age of the stellar population

The rate of mass return from stars has a dependence on the age of the stellar population, roughly as  $\propto t^{-1.3}$  after an age of  $\sim 2$  Gyrs (e.g., Ciotti et al. 1991). A population age difference from galaxy to galaxy then leads to a difference in the stellar mass return rate, that can be comparable to that estimated for variations in the inner galactic structure in the previous Sect. 4.1. For example, according to the evolutionary population synthesis models of Maraston (2005), the mass return rate of a simple stellar population with a Kroupa or Salpeter Initial Mass Function is larger than at an age of 11 Gyr by a factor of  $\sim 1.5$  at 8 Gyr,  $\sim 2.3$  at 6 Gyr and significantly larger for ages  $< 3$  Gyrs: by a factor of  $\sim 9$  at 2 Gyrs, and a factor of  $\sim 20$  at 1 Gyr. Most early type galaxies of the local universe with  $M_V < -19$ , as for most the sample in tab. 1, have ages between 3 and 14 Gyrs, based on single population evolutionary models applied to spectral line indices referring to the central galactic region (i.e., within  $R_e/10$  or  $R_e/8$ ; Thomas et al. 2005, Denicolò et al. 2005); therefore age variations can contribute to the wide variation of  $L_{\text{X,nuc}}$  shown by figs. 1–3 but they will not account for the bulk of it. Age measurements are available from the references above for  $\sim 40\%$  of the sample considered here; using them,  $L_{\text{X,nuc}}$  shows no clear trend with age, but instead a constant range of  $\sim 3$  orders of magnitude at all ages from 3 to 14 Gyr (fig. 8, left panel). At smaller ages, a couple of the lowest- $L_{\text{B}}$  galaxies in the sample (NGC221 and NGC3412) with their  $L_{\text{X,nuc}} < 10^{38}$  erg s<sup>-1</sup> extend the  $L_{\text{X,nuc}}$  range further towards lower values. Even though the subsample in fig. 8 (left panel) is small and has a bias towards the more quiescent galaxies, it suggests that the bulk of the  $L_{\text{X,nuc}}$  variation in figs. 1–3 is not related to age, consistent with the estimate above of modest variations (within a factor of a few) in the stellar mass return rate for ages  $> 3$  Gyr. Numerical models of the evolution of the nuclear activity in early type galaxies over their whole lifetime predict a larger frequency of nuclear outbursts in the past, determined by the larger mass return rate (Ciotti et al. 2010), and this should produce an increasing presence of high  $L_{\text{X,nuc}}$  values going towards smaller ages. Given that in these models the duty cy-

<sup>5</sup> Note that the mass within the central few hundreds of pc is a small fraction ( $< 0.1$ ) of the total stellar mass (Kormendy et al. 2009), so that galaxies may have a very similar total luminosity or  $M_{\text{BH}}$  (e.g., in figs. 1 and 2) but different masses at the center.

<sup>6</sup> According to the most recent characterization of the central light profiles of early type galaxies in Virgo, cusp galaxies are described by a Sérsic profile with  $n < 3$  plus an additional extra-light at the center with respect to it (Kormendy et al. 2009). Therefore the above calculations give a correct estimate for the variation of the central mass of core galaxies with different  $r_b$ , but only an approximate estimate for the variation between cusp and core galaxies.

cle of the nuclear activity is small ( $\sim 5 \times 10^{-3}$  of the past 8.5 Gyr), far larger samples are needed to test this prediction in a quantitative way.

Following *GALEX* observations, a small fraction ( $\sim 10\%$ ) of early type galaxies of the local universe has been discovered to have undergone a recent ( $< 1 - 2$  Gyr old) starformation episode (Donas et al. 2007). For very large samples, near UV photometry from *GALEX* in conjunction with the SDSS optical photometry has provided colors indicative of low levels (few percent of the total stellar mass) of recent starformation (age  $< 1$  Gyr) in  $\gtrsim 30\%$  of early type galaxies of low/intermediate mass ( $\sigma < 200 \text{ km s}^{-1}$ ; e.g., Schawinski et al. 2007). It is interesting then to check whether this phenomenon is related to accretion and  $L_{X,\text{nuc}}$ . Coming to studies of specific objects, as the SAURON sample including a representative selection of early type galaxies of the local universe, a *GALEX* study revealed recent starformation in  $\approx 15\%$  of them, again all with  $\sigma < 200 \text{ km s}^{-1}$  (Jeong et al. 2009). The limit  $\sigma < 200 \text{ km s}^{-1}$  corresponds to  $L_B < 3 \times 10^{10} L_{B,\odot}$  for the galaxies in fig. 1, therefore this recent starformation phenomenon may be of interest for only a fraction of them. High spatial resolution optical spectroscopy of 28 early type SAURON galaxies revealed young centers (age  $< 2$  Gyr) in 6 cases, preferentially galaxies that are of low-mass and fast rotating (McDermid et al. 2006; Kuntschner et al. 2006). When considering the indicators of recent starformation for the SAURON sample quoted above, there could be a trend for the largest  $L_{X,\text{nuc}}$  to reside in galaxies with a uniformly old stellar population, typically the most massive ones, and the lowest in younger galaxies or those with a younger central component, as the kinematically distinct core in NGC4382 (see the  $L_{X,\text{nuc}}$  vs. the  $H\beta$  line strength in fig. 8, right panel, where galaxies with recent starformation found from *GALEX* or with a kinematically decoupled compact component are also evidenced). Figure 8 (right panel) suggests a decrease in accretion following a starburst episode, or a galaxy merger for which the presence of a kinematically distinct component is considered an evidence, but unfortunately these considerations are based on too few objects to draw definitive conclusions.

Summarizing, the analysis in this Section reveals that 1) at all ages from 3 to 14 Gyr  $L_{X,\text{nuc}}$  covers the same wide range of values, without a clear trend of  $L_{X,\text{nuc}}$  with age; 2) the lowest  $L_{X,\text{nuc}}$  values reside in galaxies with a younger center, recent starformation, and/or with a younger stellar component at the center, with age  $< 2 - 3$  Gyr. If any, "youth" seems to be more connected with a lower  $L_{X,\text{nuc}}$ , but the following remark is in order. Most of the cases in 2) (that is NGC221, NGC3412, NGC4150, NGC4550, NGC4459 and NGC7457, labelled in fig. 8) are also galaxies with low  $L_B$  [ $\log L_B (L_{B,\odot}) \leq 10.1$ ], and fig. 1 shows a trend of  $L_{X,\text{nuc}}$  with  $L_B$ ; therefore it cannot be concluded whether the lower nuclear emission is more linked to the galaxy size ( $L_B$ ) or to the consequences of recent starformation. The latter may plausibly have a role in causing a low  $L_{X,\text{nuc}}$ : during the major galaxy formation process the feedback from the central MBH is believed to end the starformation epoch (e.g., Croton et al. 2006), but in the subsequent evolution recurrent starformation is predicted to take place at the galactic

center, connected with the recurrent nuclear outbursts; soon after these bursts, the combined heating effects of the starburst and the central MBH drive the available gas out in a wind, ending abruptly starformation and accretion as well (Ciotti et al. 2010). It is finally interesting that among the cases in 2) there is also the bright galaxy NGC4382 [ $\log L_B (L_{B,\odot}) \sim 10.8$ ], likely a post-merger galaxy due to its kinematically decoupled component. Post-merger early type galaxies undergo a "rejuvenation" of their stellar population (e.g., Thomas et al. 2005), as also proved by X-ray binaries studies (Kim & Fabbiano 2010), and are typically hot gas poor (Fabbiano & Schweizer 1995, Brassington et al. 2007). In this case, then, heating by starformation or the dynamical effect of the interaction between galaxies on the hot gas may have emptied the galaxies and starved the nuclear activity.

#### 4.3. What determines $L_{X,\text{nuc}}$ ?

The previous Sects. 4.1 and 4.2 showed that a variation in the inner stellar structure and in central age, both strictly related to the stellar mass input rate close to the MBH, can account for a variation of  $\dot{M}_{\text{BH}}$  of a factor of  $\lesssim 10$  each; therefore they can contribute to the wide  $L_{X,\text{nuc}}$  variation at fixed  $L_B$  or  $\dot{M}_{\text{BH}}$  but cannot entirely explain it. We investigated then whether  $L_{X,\text{nuc}}$  has a dependency on the total hot gas emission on the galactic scale,  $L_{X,\text{ISM}}$ ; for galaxies hosting a large steady inflow, the latter is proportional to the accreting mass flux (e.g., Fabian 2003). For this purpose we collected the available measurements of the X-ray emission from hot gas for the galaxies in tab. 1, based on *Chandra* observations, that allow to remove best the contribution of the nucleus and of X-ray binaries (contaminating instead the  $L_{X,\text{tot}}$  values considered in Sect. 4.1, from *ROSAT* data). These gas luminosities  $L_{X,\text{ISM}}$ , for 65 of the objects in tab 1, were converted to the same (0.3–2) keV band using the spectral shape used to derive them, and to the distances in tab. 1, and then compared with  $L_{X,\text{nuc}}$  in fig. 9 (references are given in its caption). Even though less objects are present than in figs. 1 and 2, fig. 9 shows that  $L_{X,\text{nuc}}$  is detected both in gas poor and in gas rich galaxies, and on average increases with  $L_{X,\text{ISM}}$ , but with a wide variation of  $L_{X,\text{nuc}}$  of 2–4 orders of magnitude for  $\log L_{X,\text{ISM}} (\text{erg s}^{-1}) \gtrsim 39$ .

Evidently, the level of radiative output from accretion is not tightly related to fuel availability within a steady scenario, either on the circumnuclear or on the galactic scale. Alternatively, then, accretion could be intermittent due to feedback from the central MBH, that occasionally heats the surrounding gas and lowers  $\dot{M}_{\text{BH}}$  until accretion is stopped; later on cooling resumes and  $\dot{M}_{\text{BH}}$  can increase again, even above values predicted for a steady inflow, since gas that has been pushed and accumulated at large radii can fall back towards the center again (e.g., Di Matteo et al. 2003, Ciotti, Ostriker & Proga 2010). In support for this, the hot gas morphology of a large fraction of high  $L_{X,\text{ISM}}$  galaxies shows cavities, shells and shocks, often associated with radio jets and lobes, that can be attributed to past nuclear outbursts, taking place every few  $10^6 - 10^8$  yrs (e.g., Forman et al. 2005, Allen et al. 2006, Diehl & Statler 2008, Baldi et al. 2009). The large spread in  $L_{X,\text{nuc}}$  could then be

produced by the activity cycle, where  $L_{X,nuc}$  is regulated by the joint actions of feedback and fuel availability.

In addition to heating from feedback, the  $\dot{M}_{BH}$  reaching the MBH could be regulated by another phenomenon, for which there are both theoretical and observational evidences. In RIAFs, only a small fraction of the gas supplied may actually fall on to the MBH, and the binding energy it releases may be transported radially outward and drive away the remainder in a wind (Blandford & Begelman 1999). The loss of a large fraction of the accretion flow is also possible due to angular momentum (Proga & Begelman 2003a) or a weak magnetic field (Proga & Begelman 2003b, Hawley & Balbus 2002). On the observational side, detailed studies of ellipticals based on *HST* and *Chandra* to estimate the accretion radius  $r_a$ , the mass accretion rate within  $r_a$  and  $L_{X,nuc}$ , concluded that for many of them  $L_{X,nuc}$  is so low that most of the available gas within  $r_a$  cannot reach the MBH, even when allowing for a low radiative efficiency (Fabbiano et al. 2004; Pellegrini 2005b; Soria et al. 2006b; Ho 2009). This "fuel overabundance" problem has been best investigated for Sgr A\*, where the X-ray and radio results imply outflows or convection close to the MBH (Baganoff et al. 2003). The possibility of a large mass loss for the accretion flow entering  $r_a$  before it reaches the MBH could be another factor accounting for the wide variation in  $L_{X,nuc}$ , if taking place in different proportions at fixed  $\dot{M}_{BH}$ . It would also help explain the mild (if any) sensitivity of  $L_{X,nuc}$  to different circumnuclear fuel productions discussed in Sects. 3 and 4.1, since the possibility of a large accretion flow depletion overcomes the role of cusps in determining  $\dot{M}_{BH}$ . A variation in the fraction of the accreting mass at  $r_a$  that effectively reaches the MBH could have already been observed: together with the "fuel overabundance" cases quoted above, in some hot gas rich galaxies with cavities the mass lost by the accretion flow on its way to the MBH cannot be large: from the energy input by feedback to their hot coronae, a high efficiency was found ( $\sim 1/5$ ) for the conversion into jet power of the accretion power  $L_{acc} \sim 0.1\dot{M}_{BH}c^2$ , where  $\dot{M}_{BH}$  is the gas mass entering  $r_a$  assuming a Bondi rate (Allen et al. 2006).

Finally, in figs. 1–3 there seems to be no gap in  $L_{X,nuc}$  and  $L_{X,nuc}/L_{Edd}$  between the brightest objects, that are a few Seyferts, and the other more radiatively quiescent objects. If the low luminosity Seyferts in this sample share the same accretion mechanism of the brighter Seyferts that are classified as classical AGNs, i.e., they are powered by a standard thin accretion disk plus hot corona (Maoz 2007; Panessa et al. 2007), then there must be a smooth transition from radiatively efficient to inefficient accretion. This may indicate a gradual changeover from a pure RIAF to an inner RIAF plus an outer thin disk, to a thin disk plus corona system (as suggested, e.g., by Ho 2008 for the Palomar sample). A continuous distribution in nuclear X-ray emission from  $10^{38}$  to  $10^{42}$  erg s $^{-1}$  was also found for the sample of nearby galaxies, of type Sa or later (Zhang et al. 2009).

#### 4.4. The radio and X-ray properties of nearby nuclei

We discuss here the different behavior of  $L_{X,nuc}$  and the core 5 GHz luminosity  $L_{R,core}$  with respect to  $\gamma$  (Sect. 3.1). The trend in the  $L_{R,core}$  versus  $\gamma$  plot (fig. 6)

is similar to the L-shape in the plot of the total soft X-ray emission  $L_{X,tot}$  versus  $\gamma$  (Pellegrini 1999, 2005a): core galaxies span a large range of soft X-ray emission, from the lowest to the highest values observed, while cusp galaxies are confined below  $L_{X,tot} \sim 10^{41}$  erg s $^{-1}$ . The relationship was explained with the core profile being characteristic of the more massive galaxies, often centrally located in groups and clusters, and then with the most favorable conditions to retain the hot gas.

The similar trends of  $L_{R,core}$  and  $L_{X,tot}$  with respect to  $\gamma$  are not unexpected, given that these two quantities correlate each other (Fabbiano et al. 1989). The L-shape that they show with respect to cusps could then be produced in both cases by the hot gas, determining it directly  $L_{X,tot}$  and being also essential for jet confinement and propagation (e.g., Worrall 2002, Kaiser 2009). In fact many of the core galaxies in fig. 6 have a radio morphology with well developed jets and lobes, or an extended radio structure indicative of a collimated outflow (Capetti & Balmaverde 2006), and the VLA radio luminosities include a contribution from the jet components. When  $L_{R,core}$  and  $L_{X,ISM}$  are above their respective thresholds, then, galaxies have the most dense coronae and the related action of confinement is more efficient. An additional link between the hot gas and the radio emission could be due to a higher accretion rate produced by a higher gas cooling rate  $L_{X,ISM}$  (as already suggested previously, Fabbiano et al. 1989; Mittal et al. 2009). Likely both actions are at work, that is a higher hot gas content provides both a more effective confinement and a higher accretion rate. The latter should of course produce also a higher  $L_{X,nuc}$ , and indeed the investigation performed here (fig. 9) shows a correlation between the nuclear luminosity  $L_{X,nuc}$  and  $L_{X,ISM}$ . The L-shape, though, is present only with respect to  $L_{R,core}$ , not  $L_{X,nuc}$  (fig. 6), probably because the action of confinement is more important for  $L_{R,core}$  than  $L_{X,nuc}$ . However, a more tight relationship between the (Bondi) accretion rate and the outcome of accretion has been found considering the jet power rather than the nuclear luminosities [Sect. 4.3; see also the lack of significant correlation between  $L_{X,nuc}$  and the Bondi rate, Pellegrini (2005b), Merloni & Heinz (2007)] since in nearby low luminosity or almost quiescent nuclei the output of accretion is dominated by the kinetic rather than the radiative power [Körding et al. 2006, Allen et al. 2006, Merloni & Heinz (2007)]. An implicit consequence of the different trend of the radio and nuclear X-ray luminosities in fig. 6 is that the  $L_{R,core}/L_{X,nuc}$  ratio should have the largest values among core galaxies, and keep below a threshold for power law galaxies. In fact, power law galaxies tend to be radio quiet and core galaxies radio loud, when using the radio-loudness parameter  $R_X = L(5 \text{ GHz})/L(2\text{--}10 \text{ keV})$  of Terashima & Wilson (2003) [see also Capetti & Balmaverde (2006); Panessa et al. (2007)].

Finally, it seems (fig. 6) that only core galaxies can reach the highest  $L_R$  and possess a conspicuous radio activity cycle. An activity cycle in cusp galaxies may take place, but with a variation of the radio emission that keeps within a smaller range, perhaps because of a rapid jet failure due to the lack of dense confining gas. For example in the hot gas poor NGC821 a mini-jet in the nuclear region has been possibly discovered in the radio (Pellegrini et al. 2007b). Another possibility is

given by the fact that cusp galaxies are on average less massive, and the duty cycle likely increases with galaxy mass, because single outbursts have greater impact in less massive systems (Ciotti et al. 2010), which then are "on" for a shorter time. Evidence for this is being found from a large sample of hot gas coronae studied with *Chandra*, where the duty cycle seem to increase from  $< 10\%$  in the less luminous galaxies with less massive hot gas halos to  $> 50\%$  in the most luminous ones (Nulsen et al. 2009).

## 5. CONCLUSIONS

In this work measurements or upper limits have been collected for the hard X-ray emission at the nucleus of 112 early type galaxies (E and S0) of the local universe (within 67 Mpc).  $L_{X,nuc}$  derives from *Chandra* data for 94% of the nuclei, and the sample includes all the available measurements of  $L_{X,nuc}$  (29 cases) for galaxies with the above characteristics and a direct estimate of the  $M_{BH}$  (38 objects). Using also  $M_{BH}$  from the  $M_{BH} - \sigma$  relation, and the inner stellar profile (slope  $\gamma$  and break radius  $r_b$ ) measured with *HST* for 81 galaxies, the relationships between  $L_{X,nuc}$  and  $M_{BH}$ , the central stellar structure, the central age, the radio and the soft X-rays (hot gas) luminosities have been investigated, with the following results:

- $L_{X,nuc}$  increases on average with  $L_B$  and  $M_{BH}$ , with a wide variation of  $L_{X,nuc}$  and  $L_{X,nuc}/L_{Edd}$ , up to 4 orders of magnitude, at any fixed galactic  $L_B > 6 \times 10^9 L_{B,\odot}$  or  $M_{BH} > 10^7 M_{\odot}$ . Cusp and core galaxies both cover the whole large range of  $L_{X,nuc}$ , without a clear trend with  $\gamma$  or  $r_b$ . Most nuclei have an Eddington ratio  $-9 < \log(L_{X,nuc}/L_{Edd}) < -5$ , the brightest ones (with  $\log(L_{X,nuc}/L_{Edd}) \sim -4$ ) are four Seyfert nuclei. The  $L_{X,nuc}/L_{Edd}$  is highest at the lowest  $M_{BH}$ , and shows an increase of its highest values with increasing "cuspiness" ( $\gamma$ ).

- Accretion in these MBHs may have entered the radiatively inefficient regime, where  $L_{X,nuc}$  scales as the mass accretion rate  $\dot{M}_{BH}^2$  at fixed  $M_{BH}$ ; therefore reasons for  $\dot{M}_{BH}$  variations explaining the wide range of observed  $L_{X,nuc}$  at fixed  $L_B$  (or  $M_{BH}$ ) are searched for. In a scenario where accretion is (quasi) steady,  $\dot{M}_{BH}$  could vary because of a different inner galactic structure, that determines the amount of mass shed by stars in the circumnuclear region and then available for accretion. The lack of a clear trend of  $L_{X,nuc}$  with  $\gamma$  and  $r_b$ , and the weak evidence for an increase of  $L_{X,nuc}/L_{Edd}$  with cuspiness, indicate that differences in the inner galactic structure do not have the dominant effect on  $L_{X,nuc}$ . In fact the circumnuclear fuel production rate is estimated to vary more than a factor of a few only when the inflowing region is small (of the order of the accretion radius) and for large differences in  $r_b$ ; in agreement with this, for galaxies with presumably a small inflowing region, a trend for  $L_{X,nuc}$  to decrease for increasing  $r_b$  seems to be present.

- The stellar mass return rate depends also on the age of the stellar population, but  $L_{X,nuc}$  covers the same wide range of values at all central ages from 3 to 14 Gyr; "youth", indicated by a younger center, recent starformation, and/or a younger stellar component at the center (of ages  $< 2 - 3$  Gyr), seems to be more connected with a lower  $L_{X,nuc}$ . An explanation could be that the heating by starformation or the dynamical effect of the

merging process on the hot gas drive the available gas out in a wind, ending abruptly the starformation and accretion. However, this finding remains an indication, because of the trend of  $L_{X,nuc}$  with  $L_B$  and the small number of galaxies with information about recent starformation episodes.

- $L_{X,nuc}$  on average increases with the total hot gas emission  $L_{X,ISM}$ , but the relation is not tight: it shows a large variation of 2–3 orders of magnitude both at the lowest and highest gas contents. Nuclear emission at the highest detected levels for this sample ( $L_{X,nuc} \sim 10^{40} - 10^{41} \text{ erg s}^{-1}$ ) is present even when the gas content is low, and  $L_{X,nuc}$  at the lowest levels ( $\sim 10^{38} - 10^{39} \text{ erg s}^{-1}$ ) can be found at gas luminosities differing by 3 orders of magnitude.

- The mild sensitivity of  $L_{X,nuc}$  to the circumnuclear and global hot gas contents, and its large variation, finds two possible explanations, both of which go in the sense of overcoming the importance of fuel availability : 1) the gas is heated due to feedback from the MBH, which could be a phenomenon not limited to high  $L_{X,ISM}$  galaxies, or 2) only a small fraction of the mass entering the accretion radius actually reaches the MBH, as in RIAF models with winds/outflows, and this fraction can vary largely at fixed  $M_{BH}$ .

- A sub-sample of galaxies shows an already known trend by which cusp galaxies are confined below a threshold in the VLA 5 GHz central luminosity  $L_{R,core}$ , while core galaxies span a large range of  $L_{R,core}$ ; this subsample does not show a similar trend of  $L_{X,nuc}$  with the central light profile. The  $L_{R,core}$  behavior is instead similar to that of the total soft X-ray emission with respect to  $\gamma$ ; the hot gas could then be responsible both for the soft X-ray emission and the jet confinement and propagation. While core galaxies can possess a conspicuous radio activity cycle, in cusp galaxies the variation of the radio emission keeps within a smaller range, because of a rapid jet failure due to the lack of a dense confining medium, or a smaller duty cycle, being these galaxies on average less massive systems.

The referee is thanked for useful comments. I acknowledge use of the NASA Extragalactic database (NED), operated by the Jet Propulsion Laboratory, California Institute of Technology, and of the Hyperleda database (<http://leda.univ-lyon1.fr/>).



**Table 1**  
The nuclear properties of the sample of early type galaxies.

Name	$B_T^0$ (mag)	d (Mpc)	Ref	$\gamma$	$\log L_{X,nuc}$ ( $\text{erg s}^{-1}$ )	Ref	$\log M_{BH}$ ( $M_\odot$ )	Ref
(1)	(2)	(3)	(4)	(5)	(6)	(7)	(8)	(9)
NGC221	8.22	0.81	a	.....	35.95	1	6.47	2
NGC404	10.94	3.3	a	.....	36.84	2	5.39	1
NGC474	12.20	29.3	b	0.37	38.41	3	7.88	1
NGC507	12.23	63.8	b	0.00	<39.71	4	8.96	1
NGC524	11.01	24.0	a	0.03	38.60	3	8.63	1
NGC720	11.05	27.7	a	0.06	38.90	5	8.56	1
NGC821	11.25	24.1	a	0.10	<38.37	6	7.60	2
NGC1023	9.29	11.4	a	0.74	38.13	7	7.64	2
NGC1052	11.32	19.4	a	0.18	41.20	3	8.29	1
NGC1316	9.29	21.5	a	0.35	39.30	8	8.44	1
NGC1331	14.15	24.2	a	.....	38.13	9	6.09	1
NGC1332	11.03	24.2	a	.....	<38.77	9	9.04	1
NGC1380	10.80	17.6	a	1.0 <sup>a</sup>	40.10	10	8.40	1
NGC1395	10.48	24.1	a	.....	39.06	11	8.59	1
NGC1399	10.35	20.0	a	0.12	<38.96	12	8.68	2
NGC1404	10.81	21.0	a	.....	40.57	10	8.50	1
NGC1407	10.38	28.8	a	.....	<39.14	14	8.76	1
NGC1549	10.61	19.7	a	.....	38.46	13	8.25	1
NGC1553	10.20	18.5	a	0.74	40.22	2	8.02	1
NGC1600	11.68	57.4	b	-0.03	<39.49	15	9.11	1
NGC1700	11.78	40.6	b	-0.10	38.84	13	8.54	1
NGC2110	11.85	31.3	c	.....	42.47	16	8.65	1
NGC2300	11.73	30.4	b	0.07	40.96	10	8.69	1
NGC2434	11.25	21.6	a	0.75	<37.58	10	8.10	1
NGC2865	12.05	37.8	a	.....	39.40	17	7.97	1
NGC2974	11.61	21.5	a	0.62	40.32	10	8.53	1
NGC3115	9.87	9.7	a	0.52	38.73	7	8.96	2
NGC3125	13.01	13.4	c	.....	37.60	18	5.91	1
NGC3193	11.86	34.0	a	0.01	<39.74	10	8.17	1
NGC3226	12.22	23.6	a	1.0 <sup>a</sup>	40.80	3	8.17	1
NGC3245	11.53	20.9	a	0.73 <sup>a</sup>	39.00	3	8.32	2
NGC3309	12.15	56.5	c	.....	<39.14	19	8.67	1
NGC3311	12.40	52.7	c	.....	<39.08	19	8.10	1
NGC3377	10.98	11.2	a	0.03	38.24	20	8.02	2
NGC3379	10.11	10.6	a	0.18	38.12	21	8.04	2
NGC3384	10.76	11.6	a	0.71	38.11	7	7.24	2
NGC3412	11.30	11.3	a	.....	37.56	7	7.06	1
NGC3414	11.93	25.2	a	0.83	39.90	3	8.52	1
NGC3516	12.32	35.0	c	0.97 <sup>a</sup>	42.60	16	7.82	1
NGC3557	10.92	45.7	a	0.00 <sup>a</sup>	40.24	22	8.77	1
NGC3585	10.52	20.0	a	0.31	38.93	23	8.51	2
NGC3607	10.83	22.8	a	0.26	38.80	3	8.14	2
NGC3608	11.46	22.9	a	0.09	38.21	3	8.32	2
NGC3923	10.39	22.9	a	.....	39.73	10	8.65	1
NGC3945	11.56	19.9	b	-0.06	39.00	3	8.00	1
NGC3998	11.32	14.1	a	0.80 <sup>a</sup>	41.46	24	8.36	2
NGC4026	11.59	13.6	a	0.68 <sup>a</sup>	38.41	18	8.26	2
NGC4036	11.41	23.3	c	0.36 <sup>a</sup>	39.05	3	8.06	1
NGC4111	11.60	15.0	a	0.50 <sup>a</sup>	40.40	3	7.71	1
NGC4125	10.53	23.9	a	.....	38.70	3	8.45	1
NGC4143	11.75	15.9	a	0.59	39.98	2	8.35	1
NGC4150	12.41	13.7	a	0.58	<37.43	7	6.76	1
NGC4168	11.92	37.3	b	0.17	<39.07	22	8.09	1
NGC4203	11.66	15.1	a	0.62 <sup>a</sup>	40.08	7	7.87	1
NGC4261	11.24	31.6	a	0.00	41.10	3	8.72	2
NGC4278	10.91	16.1	a	0.06	40.11	25	8.53	1
NGC4291	12.20	26.2	a	0.01	40.57	10	8.53	2
NGC4342	13.36	11.6	c	.....	38.70	18	8.37	2
NGC4365	10.39	20.4	a	0.07	38.25	26	8.65	1
NGC4374	9.89	18.4	a	0.13	39.50	3	9.20	2
NGC4382	9.88	18.4	a	0.00	<37.93	26	8.04	1
NGC4387	12.82	21.4	a	0.10	<38.48	26	7.12	1
NGC4406	9.71	17.1	a	-0.04	<38.34	26	8.51	1

Name	$B_T^0$ (mag)	d (Mpc)	Ref	$\gamma$	$\log L_{X,nuc}$ ( $\text{erg s}^{-1}$ )	Ref	$\log M_{BH}$ ( $M_\odot$ )	Ref
(1)	(2)	(3)	(4)	(5)	(6)	(7)	(8)	(9)
NGC4417	11.96	16.7	a	0.71	<38.26	26	7.55	1
NGC4435	11.37	17.4	a	0.33 <sup>a</sup>	38.45	26	7.81	1
NGC4458	12.77	17.2	a	0.16	<38.07	26	7.08	1
NGC4459	11.25	16.1	a	0.66 <sup>a</sup>	38.40	3	7.85	2
NGC4464	13.45	16.5	a	.....	38.39	26	7.45	1
NGC4467	14.79	17.2	a	.....	<38.45	26	6.42	1
NGC4472	9.16	16.3	a	0.01	<38.67	12	8.89	1
NGC4473	10.91	15.7	a	-0.07	<38.14	7	8.08	2
NGC4478	12.04	18.1	a	-0.10	<38.49	26	7.59	1
NGC4486	9.47	16.1	a	0.27	40.80	3	9.53	2
NGC4486B	14.18	16.9	a	.....	37.91	20	7.95	1
NGC4494	10.57	17.1	a	0.52	38.80	3	7.74	1
NGC4550	12.31	15.9	a	.....	<38.37	7	6.98	1
NGC4552	10.49	15.4	a	-0.10	39.20	3	8.63	1
NGC4564	11.81	15.0	a	0.80	38.45	20	7.78	2
NGC4570	11.62	17.9	a	.....	38.18	26	8.12	1
NGC4578	12.24	18.5	a	.....	< 38.36	26	7.35	1
NGC4589	11.55	22.0	a	0.21	38.90	3	8.43	1
NGC4612	11.94	17.2	a	.....	38.08	26	6.24	1
NGC4621	10.52	18.3	a	0.75	38.92	7	8.44	1
NGC4636	10.29	14.7	a	0.13	<38.24	12	8.25	1
NGC4649	9.70	16.8	a	0.17	38.09	7	9.33	2
NGC4660	11.90	12.8	a	0.91	38.22	26	8.13	1
NGC4696	11.13	35.5	a	0.10	40.00	3	8.64	1
NGC4697	10.10	11.8	a	0.22	38.41	20	8.28	2
NGC4754	11.35	16.8	a	.....	38.31	26	8.09	1
NGC4759	13.75	50.7	c	.....	< 38.78	27	8.49	1
NGC5018	11.23	39.4	c	.....	< 39.41	28	8.32	1
NGC5044	11.24	31.2	a	.....	39.44	29	8.54	1
NGC5102	10.01	4.0	a	.....	36.56	18	7.58	1
NGC5128	7.28	4.2	a	0.10 <sup>a</sup>	41.88	30	8.46	2
NGC5273	12.47	16.5	a	0.37 <sup>a</sup>	40.55	31	6.60	1
NGC5283	14.15	48.7	c	.....	41.91	32	7.71	1
NGC5322	10.96	31.2	a	0.00 <sup>a</sup>	40.29	10	8.49	1
NGC5419	11.53	62.6	b	-0.10	40.82	22	9.20	1
NGC5813	11.24	32.2	a	0.05	38.80	3	8.52	1
NGC5838	11.53	22.2	b	0.93	38.99	3	8.72	1
NGC5845	13.19	25.9	a	0.51	39.07	20	8.42	2
NGC5846	10.82	24.9	a	0.00 <sup>a</sup>	40.80	3	8.54	1
NGC5866	10.66	15.3	a	0.00 <sup>a</sup>	38.30	3	7.84	1
NGC6482	11.73	58.6	c	.....	39.39	3	8.97	1
NGC7052	13.30	67.1	b	0.16	<40.28	4	8.58	2
NGC7332	11.79	23.0	a	0.62	<39.70	10	7.42	1
NGC7457	11.63	13.2	a	-0.10	37.91	18	6.58	2
NGC7619	11.70	53.0	a	-0.02	40.84	7	9.05	1
NGC7626	11.81	53.0	a	0.36	41.10	7	8.75	1
NGC7743	12.07	20.7	a	0.50	39.50	3	6.75	1
IC1459	10.86	29.2	a	-0.10	40.87	33	9.42	2
IC4296	11.24	48.8	a	0.00 <sup>a</sup>	41.20	34	9.10	1

<sup>a</sup>  $\gamma$  from the modeling with the Nuker law by Capetti & Balmaverde (2005), see Sect. 3; NGC1380 and NGC3226 are just defined cusp galaxies, for them  $\gamma = 1$  is assumed here.

Column (1): galaxy name. Col. (2): total apparent blue magnitude, corrected for galactic and internal extinction, from HyperLeda. Col. (3): distance, for  $H_0 = 70 \text{ km s}^{-1} \text{ Mpc}^{-1}$ , based on sources given in col. (4), taken with this priority: the SBF method [Tonry et al. (2001), a in col. (4); distances derived from this work are now consistent with  $H_0 = 70 \text{ km s}^{-1} \text{ Mpc}^{-1}$  after more recent Cepheid and Hubble flow recalibrations, J. Tonry 2010, private communication; for IC4296 the reference is Mei et al. 2000; for a few Virgo galaxies not in Tonry et al. (2001), the results of Blakeslee et al. (2009) have been used]; Lauer et al. (2007a) [b in col. (4)]; these authors reworked the distances in various sources to be consistent with  $H_0 = 70 \text{ km s}^{-1} \text{ Mpc}^{-1}$ ; the recession velocity corrected for Virgo infall, given by HyperLeda [c in col. (4)]. Col. (5): inner slope of stellar light profile, from Lauer et al. (2007a), except for cases marked with the apex <sup>a</sup>. Col. (6): nuclear luminosity in the 2–10 keV band, rescaled for the distance in col.(3), from the reference in col. (7) (see Sect. 2). Col. (8): central black hole mass, from the method specified in col. (9), where 1 = the  $M_{BH} - \sigma$  relation of Gültekin et al. (2009) for elliptical galaxies, 2 = a direct mass measurement with a dynamical modeling (references in Gültekin et al. 2009); when necessary, the masses have been rescaled for the distance in col. (3).

**References.** — col. (7): 1=Ho et al. 2003, 2=Eracleous et al. 2010, 3=González-Martín et al. 2009, 4=Donato et al. 2004, 5=Jeltema et al. 2003, 6=Pellegrini et al. 2007b, 7=Ho 2009, 8=Rinn et al. 2005, 9=Humphrey & Buote 2004, 10=Liu & Bregman 2005, or Liu 2008 (arXiv:0811.0804) for NGC1404, NGC2434 and NGC3923, 11=Colbert et al. (2004), 12=Loewenstein et al. 2001, 13=Diehl & Statler 2008, 14=Zhang et al. 2007, 15=Sivakoff et al. 2004, 16=Winter et al. 2009, 17=Sansom et al. 2006, 18=Zhang et al. 2009, 19=Yamasaki et al. 2002, 20=Soria et al. 2006a, 21=Brassington et al. 2008, 22=Balmaverde & Capetti 2006, 23=O’Sullivan & Ponman 2004, 24=Pellegrini et al. 2000, 25=Brassington et al. 2009, 26=Gallo et al. 2010, 27=Morita et al. 2006, 28=Ghosh et al. 2005, 29=David et al. 2009, 30=Evans et al. 2004, 31=Capetti & Balmaverde 2006, 32=Ghosh et al. 2007, 33=Fabbiano et al. 2003, 34=Pellegrini et al. 2003b.

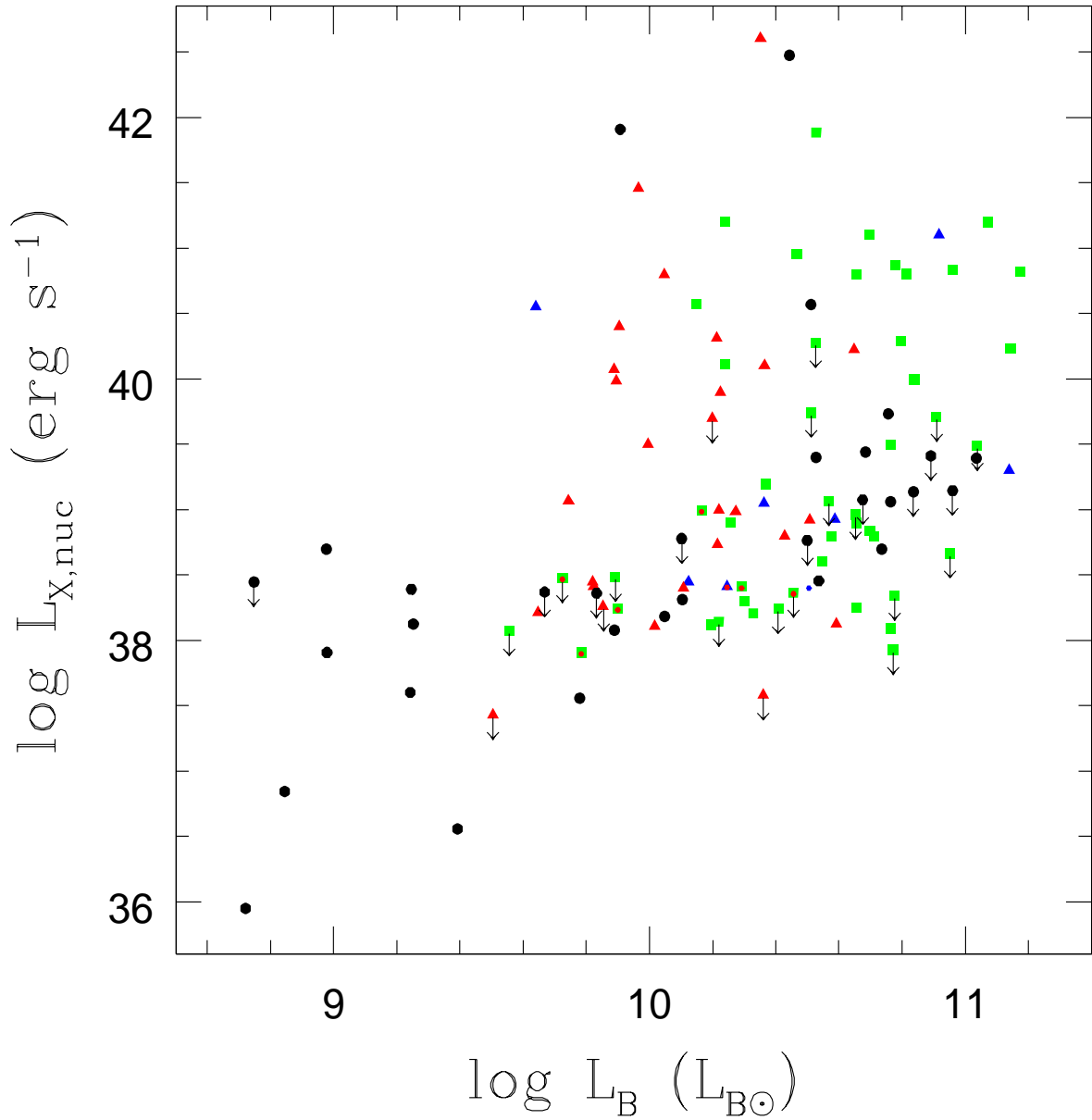


**Figure 1.** The relation between the nuclear luminosity in the 2–10 keV band  $L_{X,nuc}$  and the galactic luminosity  $L_B$  for the sample described in Sect. 2. Upper limits on  $L_{X,nuc}$  are marked by an arrow; red and blue triangles are cusp and intermediate galaxies, green squares are core ones (all according to their  $\gamma$  values in Tab. 1), unknown profiles are shown with black circles. Those 7 cases that become cusp (intermediate), when using  $\gamma'$  instead of  $\gamma$  for their classification, are marked with a red (blue) dot inside the symbol (see Sect. 2 and 3 for more details).

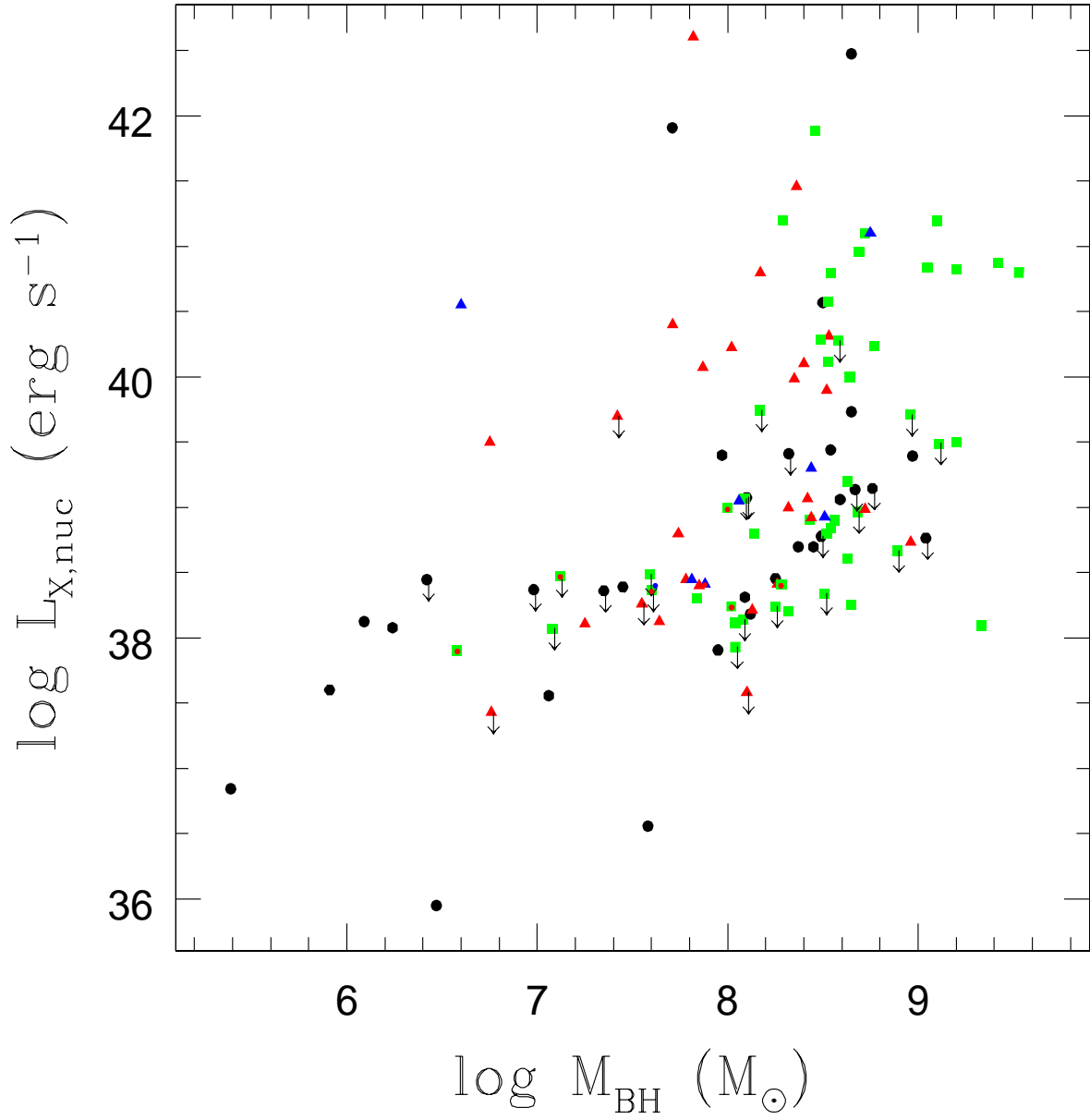


**Figure 2.** The relation between the nuclear luminosity in the 2–10 keV band  $L_{X,\text{nuc}}$  and the MBH mass  $M_{\text{BH}}$ , with symbols as in fig. 1;  $M_{\text{BH}}$  comes from direct estimates or the  $M_{\text{BH}} - \sigma$  relation, as specified in Tab. 1 (see Sects. 2 and 3 for more details).

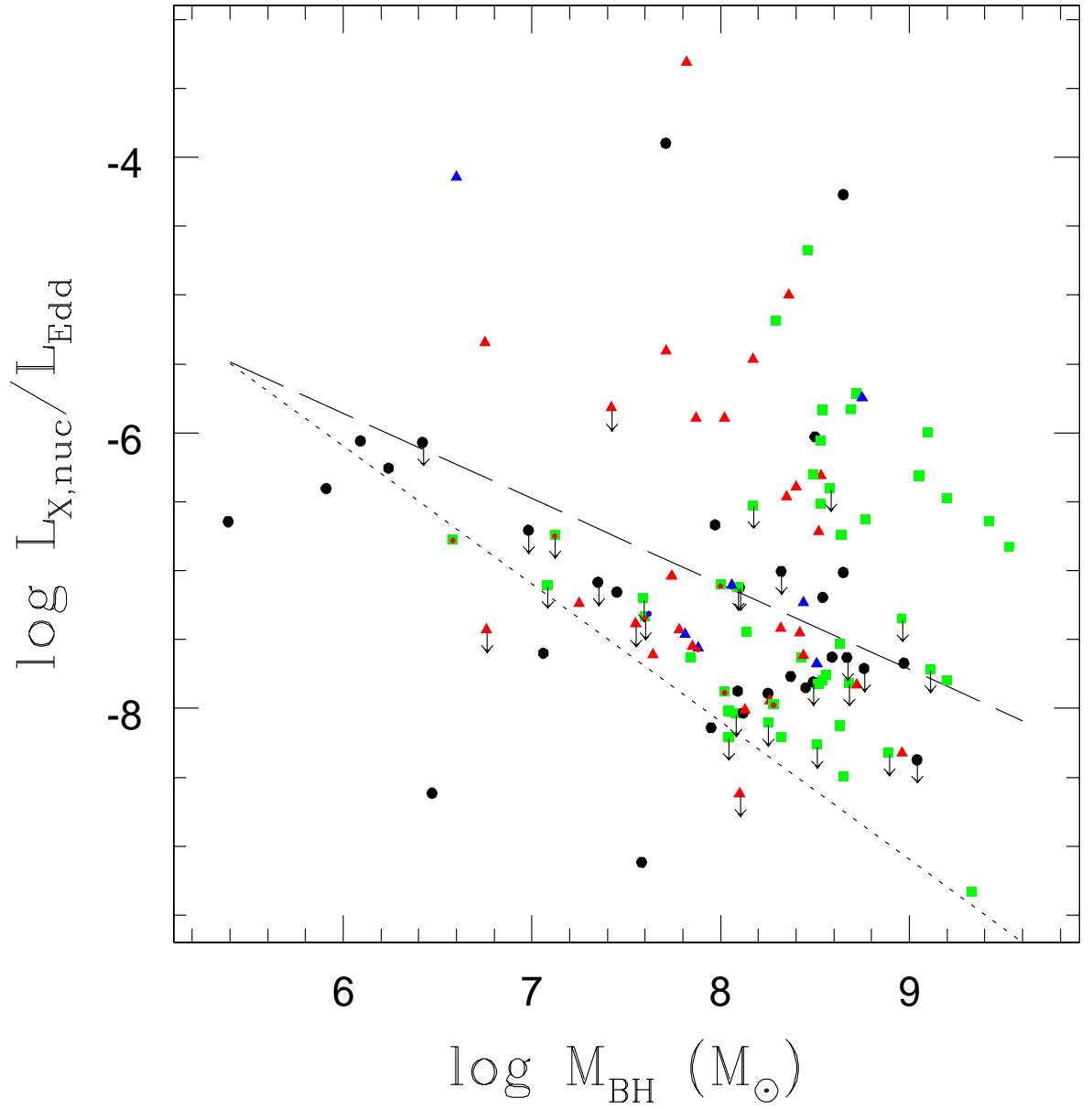


**Figure 3.** The relation between  $L_{X,nuc}/L_{Edd}$  and  $M_{BH}$ , with symbols as in fig. 1; the dashed line is the average trend found for the ACS VCS sample by Gallo et al. (2010) (see Sect. 3 for more details).

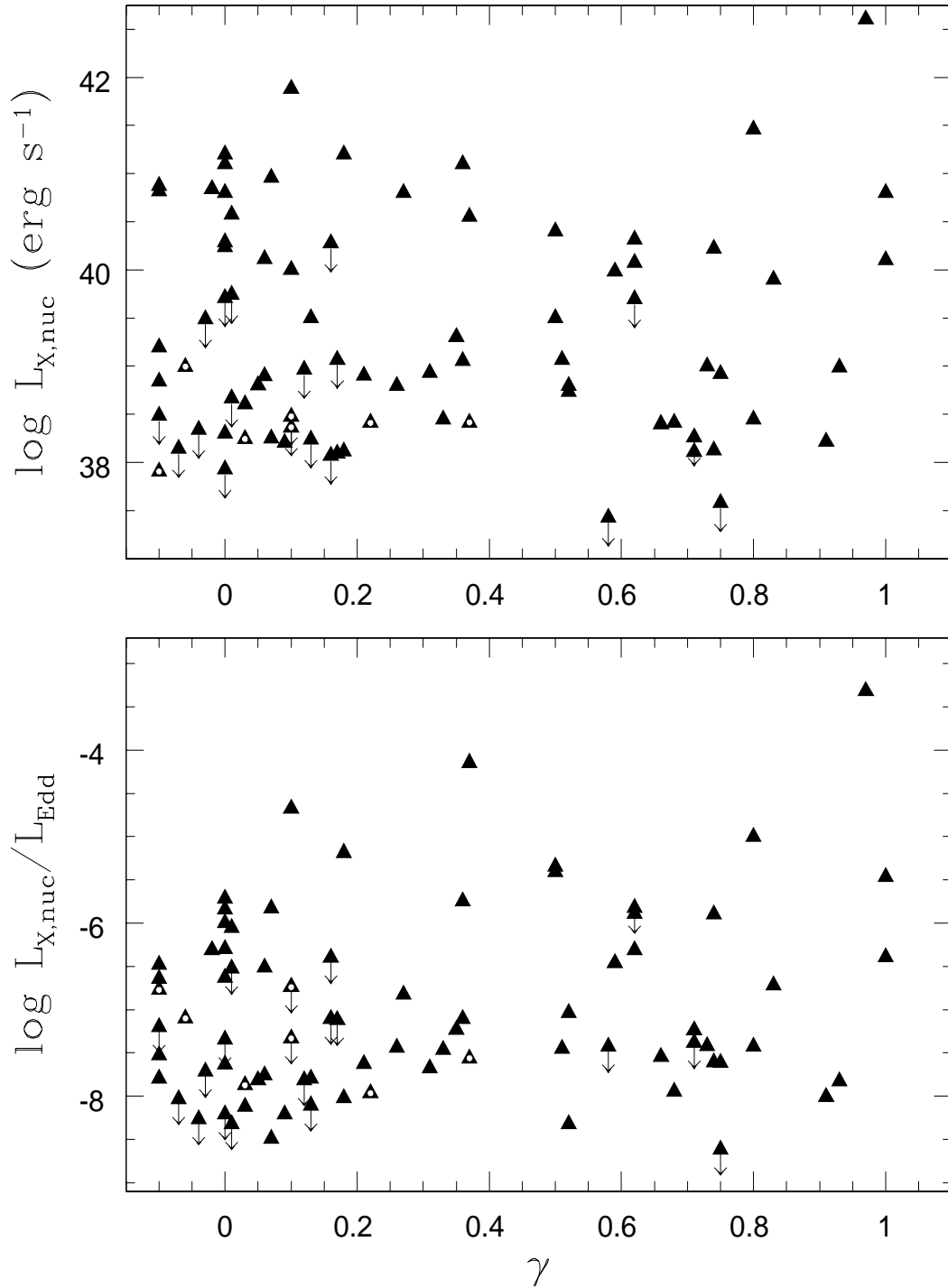


**Figure 4.** The relationships between  $L_{X,nuc}$  and the slope of the stellar light profile in the central galactic region  $\gamma$  (upper panel), and between  $L_{X,nuc}/L_{Edd}$  and  $\gamma$  (lower panel). Upper limits on  $L_{X,nuc}$  are shown with an arrow. Galaxies that change their classification from core to cusp or intermediate when using  $\gamma'$  instead of  $\gamma$  (Sect. 2) are marked with a white dot inside their symbol.

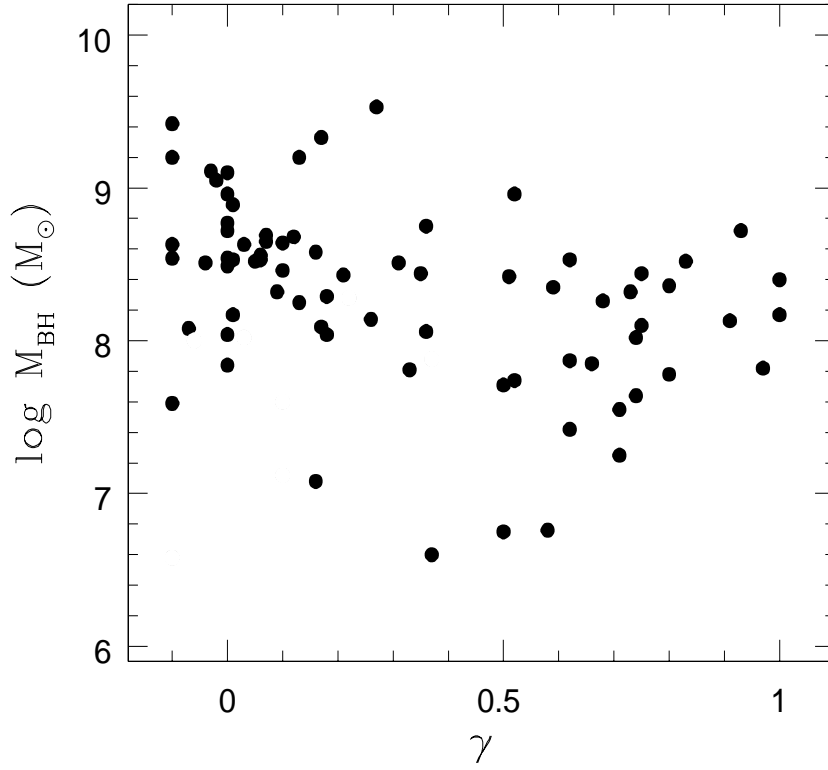


**Figure 5.** The relationships between the mass of the MBH and the slope of the stellar light profile in the central galactic region  $\gamma$  for the sample in tab. 1; the 7 galaxies that change their classification from core to cusp or intermediate when using  $\gamma'$  instead of  $\gamma$  (Sect. 2) have been excluded.

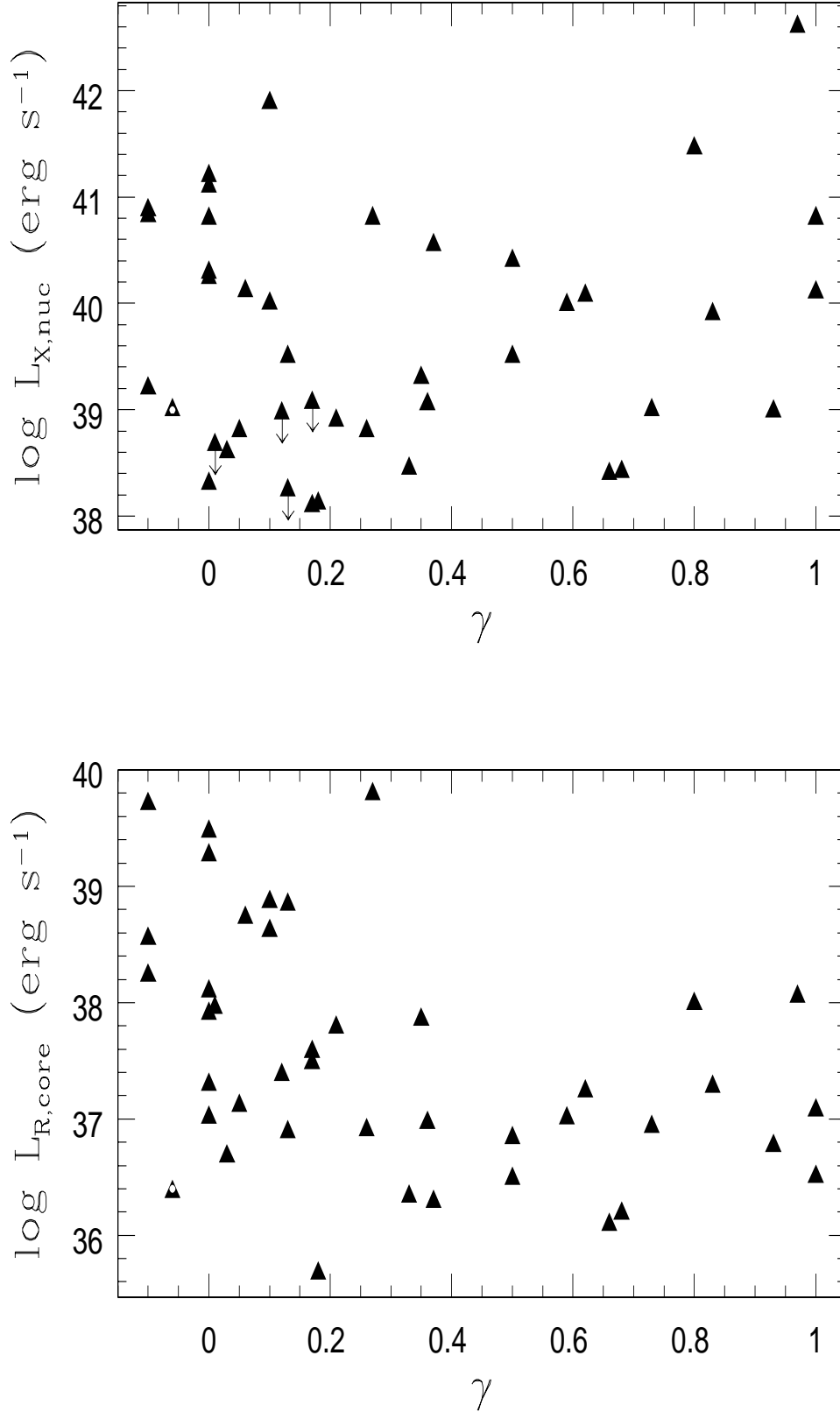


**Figure 6.** The relationship between the inner light profile shape  $\gamma$  and  $L_{X,nuc}$  (upper panel), or the core radio luminosities at 5 GHz (lower panel), for the Capetti & Balmaverde (2005) sample. The L-shaped trend with  $\gamma$  is apparent for the radio luminosity, but is absent for  $L_{X,nuc}$ . The white dot inside the symbol marks NGC3945 that becomes a cusp galaxy according to  $\gamma'$ . See Sect. 3.1 for more details.



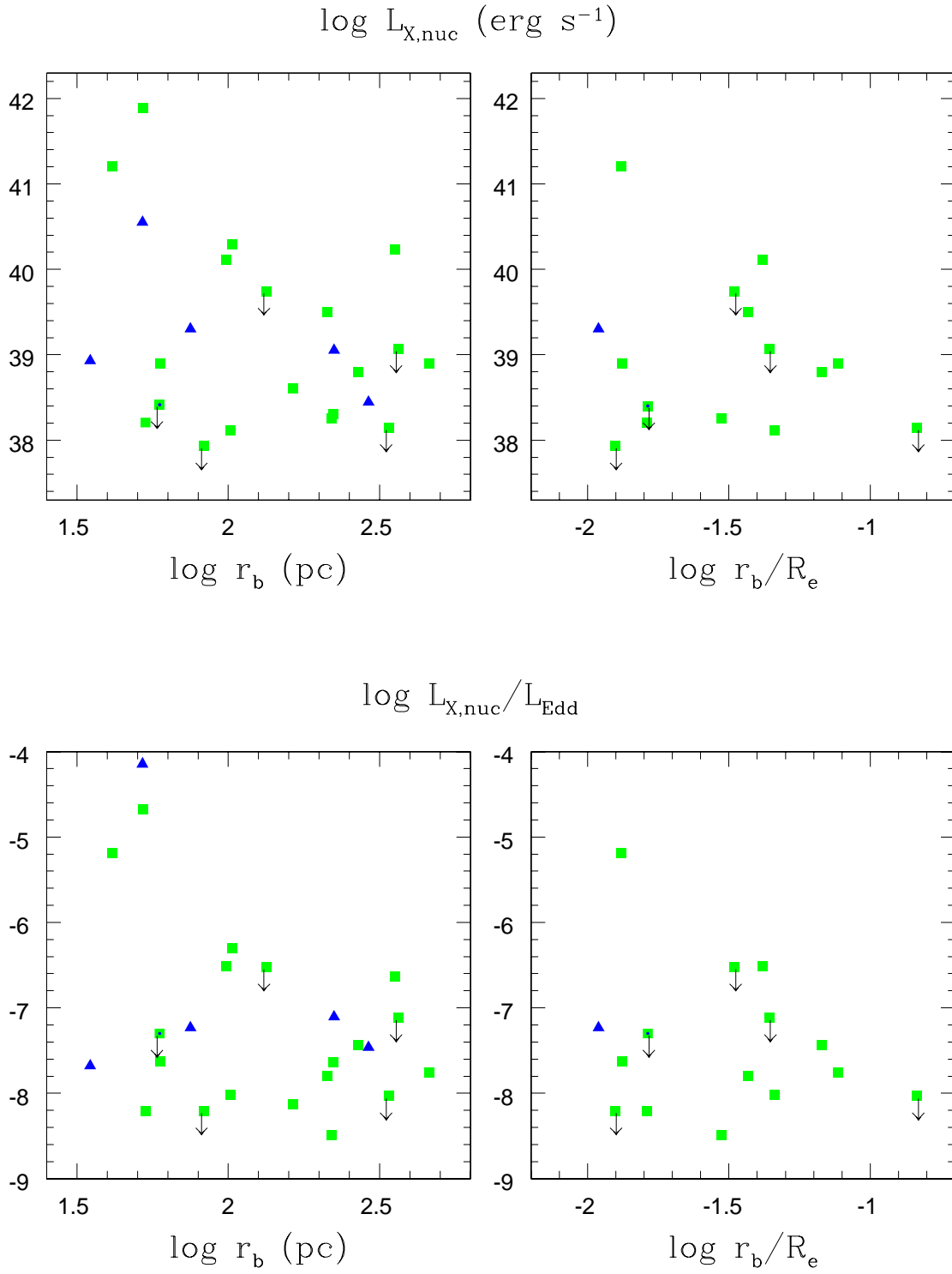


**Figure 7.**  $L_{X,\text{nuc}}$  (upper panels) and  $L_{X,\text{nuc}}/L_{\text{Edd}}$  (lower panels) versus  $r_b$  and  $r_b/R_e$  for galaxies with a low hot gas content (see Sect. 4.1).

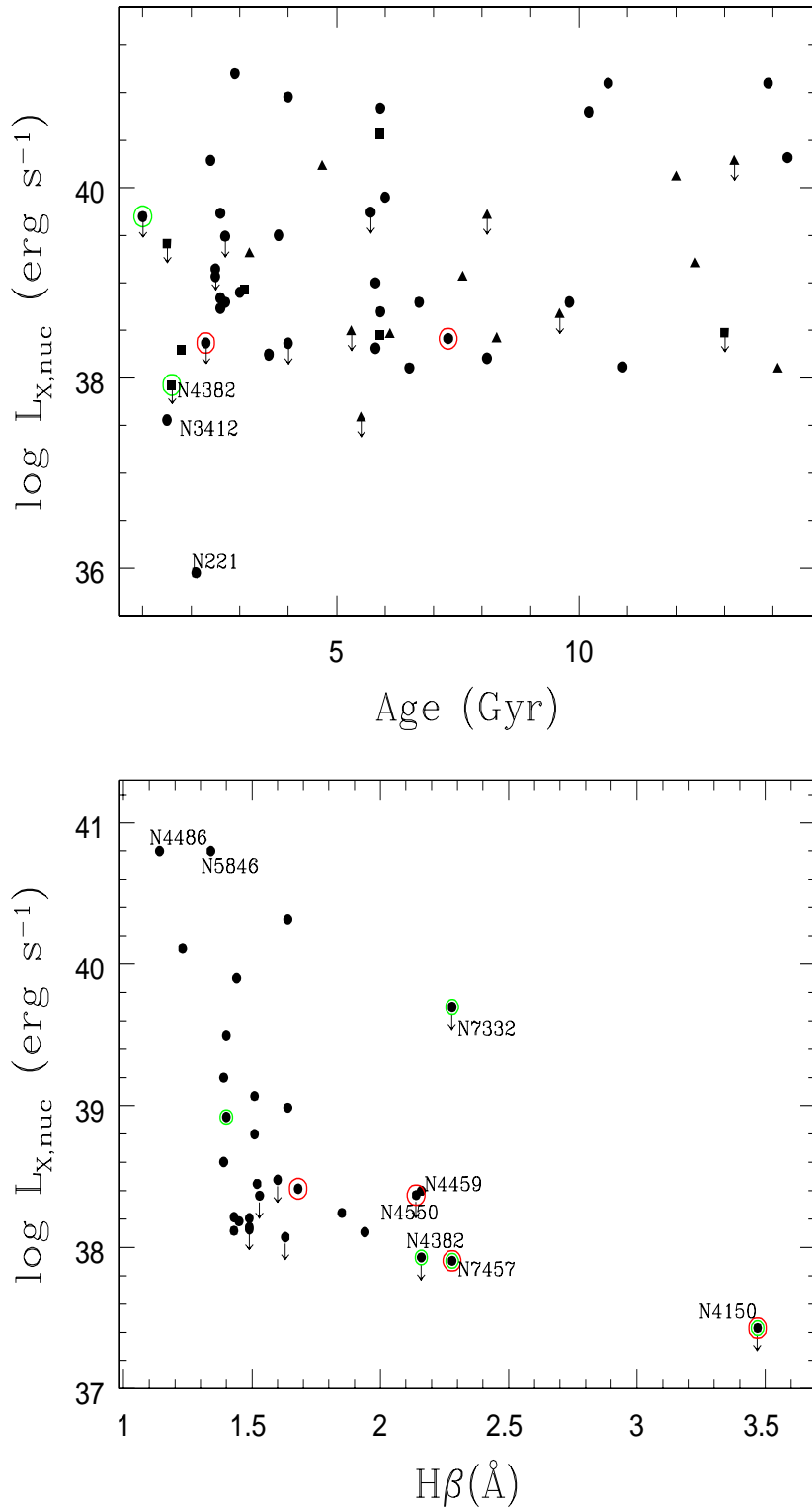


**Figure 8.**  $L_{X,nuc}$  versus stellar population age indicators derived for a central aperture of radius  $R_e/8$ : the age of stellar population synthesis models reproducing observed spectral indices, in the upper panel (circles indicate estimates by Denicoló et al. 2005, squares by Terlevich & Forbes 2002, triangles by Thomas et al. 2005 for an aperture of  $R_e/10$ ); the  $H\beta$  absorption line strength, indicative of recent starformation, in the lower panel (data from Kuntschner et al. 2006 for the SAURON sample); see Sect. 4.2 for more details. In both panels, the red circles mark the cases where recent starformation has been found from *GALEX* (Jeong et al. 2009), and the green circles the presence of kinematically distinct compact cores; in the right panel, the high  $H\beta$  line strengths of NGC4150, NGC4382, NGC7332 and NGC7457 are due to these compact components residing at their centers (McDermid et al. 2006).

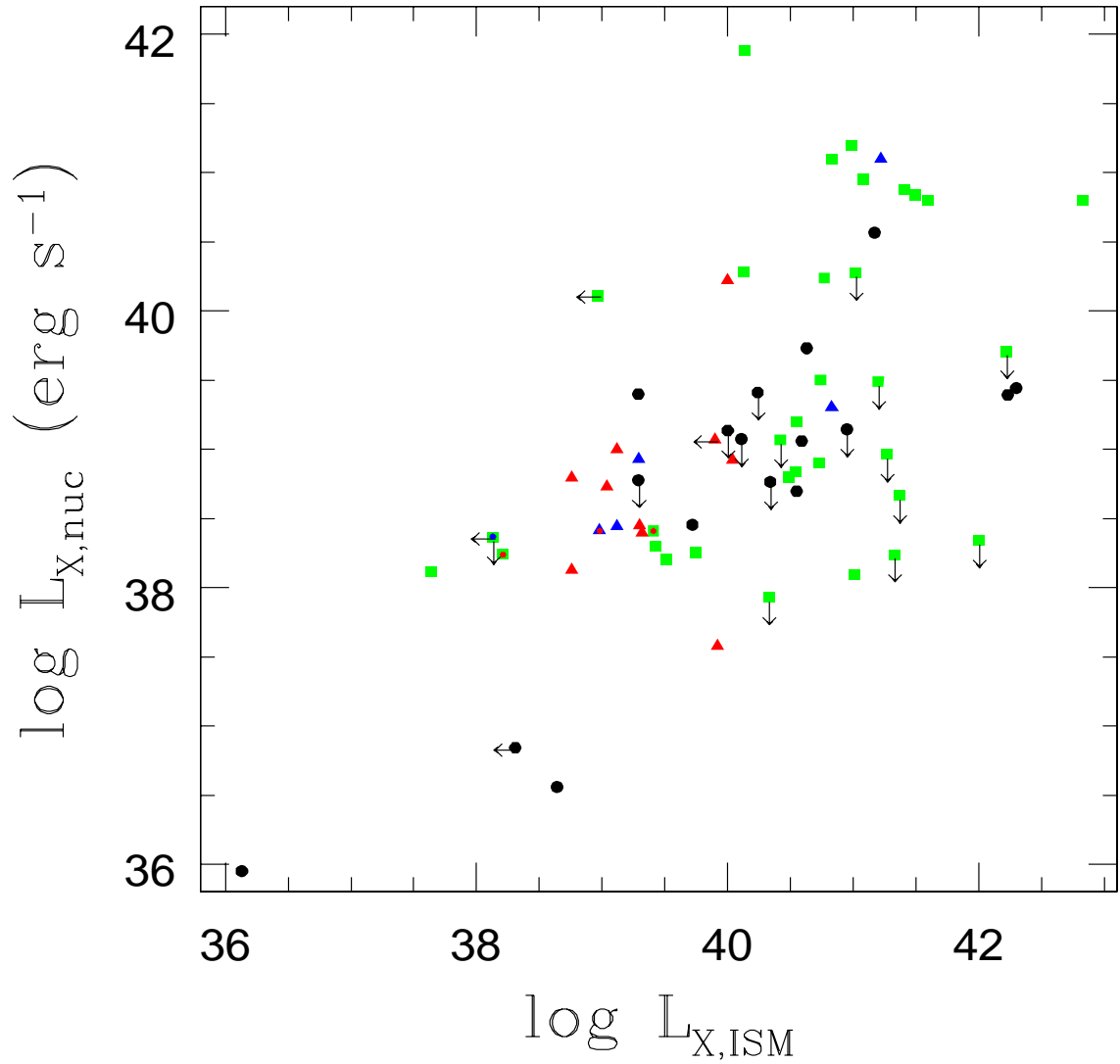


**Figure 9.** The nuclear luminosity  $L_{X,nuc}$  from tab. 1 against the X-ray luminosity of the hot ISM estimated from *Chandra* observations, from Nagino & Matsushita (2009), Memola et al. (2009), Trinchieri et al. (2008), Diehl & Statler (2008), Jeltama et al. (2008), Kim et al. (2008), Pellegrini et al. (2007a), David et al. (2006), Fukazawa et al. (2006), Finoguenov et al. (2006), Rampazzo et al. (2006), Kraft et al. (2003), Yamasaki et al. (2002). See Sect. 4.3.

## REFERENCES

- Allen, S.W., Dunn, R.J.H., Fabian, A.C., Taylor, G.B., Reynolds, C.S. 2006, *MNRAS* 372, 21
- Baganoff, F. K., Maeda, Y., Morris, M., Bautz, M. W., Brandt, W. N., Cui, W., Doty, J. P., Feigelson, E. D., Garmire, G. P., Pravdo, S. H., Ricker, G. R., Townsley, L. K. 2003, *ApJ* 591, 891
- Baldi, A., Forman, W., Jones, C., Kraft, R., Nulsen, P., Churazov, E., David, L., Giacintucci, S. 2009, *ApJ* 707, 1034
- Balmaverde, B., Capetti, A. 2006, *A&A* 447, 97
- Bender R., Surma P., Döbereiner S., Möllenhoff C., Madejsky R. 1989, *A&A* 217, 35
- Blakeslee, J. P., Jordán, Andrés, Mei, S., et al. 2009, *ApJ* 694, 556
- Blandford, R. D., Begelman, M. C. 1999, *MNRAS* 303, L1
- Brassington, N. J., Ponman, T. J., Read, A. M. 2007, *MNRAS* 377, 1439
- Brassington, N. J., Fabbiano, G., Kim, D.-W., et al. 2008, *ApJS* 179, 142
- Brassington, N. J., Fabbiano, G., Kim, D.-W., et al. 2009, *ApJS* 181, 605
- Capetti, A., Balmaverde, B. 2005, *A&A* 440, 73
- Capetti, A., Balmaverde, B. 2006, *A&A* 453, 27
- Ciotti L., D’Ercole A., Pellegrini S., Renzini A. 1991, *ApJ* 376, 380
- Ciotti, L., & Ostriker, J.P. 2007, *ApJ* 665, 1038
- Ciotti, L., Ostriker, J. P., Proga, D. 2010, in press on *ApJ* (arXiv:1003.0578)
- Colbert, E. J. M.; Heckman, T. M., Ptak, A.F., Strickland, D. K., Weaver, K. A. 2004, *ApJ* 602, 231
- Croton, D. J., Springel, V., White, S. D. M. et al. 2006, *MNRAS* 365, 11
- David, L. P., Forman, W., Jones, C. 1991, *ApJ* 369, 121
- David, L.P., Jones, C., Forman, W., Vargas, I.M., Nulsen, P. 2006, *ApJ* 653, 207
- David, L.P., et al. 2009, *ApJ* 705, 624
- Denicoló, G. Terlevich, R., Terlevich, E., Forbes, D. A., Terlevich, A. 2005, *MNRAS* 358, 813
- Diehl, S., Statler, T. S. 2008, *ApJ* 680, 897
- Di Matteo, T., Allen, S. A., Fabian, A.C., Wilson, A.S., Young, A. J. 2003, *ApJ* 582, 133
- Donato, D., Sambruna, R. M., Gliozzi, M. 2004, *ApJ* 617, 915
- Donas, J., Deharveng, J.M., Rich, R. M. et al. 2007, *ApJS* 173, 597
- Ebisuzaki, T., Makino, J., Tsuru, T.G., Funato, Y., Portegies Zwart, S., Hut, P., McMillan, S., Matsushita, S., Matsumoto, H., Kawabe, R. 2001, *ApJ* 562, L19
- Evans, D. A., Kraft, R. P., Worrall, D. M., Hardcastle, M. J., Jones, C.; Forman, W. R., Murray, S. S. 2004, *ApJ* 612, 786
- Fabbiano, G., Schweizer, F. 1995, *ApJ* 447, 572
- Fabbiano, G., Gioia, I. M., Trinchieri, G. 1989, *ApJ* 347, 127
- Fabbiano, G., Elvis, M., Markoff, S., Siemiginowska, A., Pellegrini, S., Zezas, A., Nicastro, F., Trinchieri, G., & McDowell, J. 2003, *ApJ* 588, 175
- Fabbiano, G., Baldi, A., Pellegrini, S., Siemiginowska, A., Elvis, M., Zezas, A., McDowell, J. 2004, *ApJ* 616, 730
- Faber, S.M., Tremaine, S., Ajhar, E.A., et al. 1997, *AJ* 114, 1771
- Fabian, A.C. 2003, *MNRAS* 344, L27
- Ferrarese, L., Merritt, D. 2000, *ApJ* 539, L9
- Ferrarese, L., et al. 2006, *ApJS* 164, 334
- Finoguenov, A., Davis, D. S., Zimer, M., Mulchaey, J. S. 2006, *ApJ* 646, 143
- Forman, W., Nulsen, P., Heinz, S., et al. 2005, *ApJ*, 635, 894
- Fukazawa, Y., Botoya-Nonesha, J. G., Pu, J., Ohto, A., & Kawano, N. 2006, *ApJ*, 636, 698
- Gallo, E., Treu, T., Jacob, J., Woo, J.-H., Marshall, P.J., Antonucci, R. 2008, *ApJ* 680, 154
- Gallo, E., Treu, T., Marshall, P.J., Woo, J.-H., Leipski, C., Antonucci, R. 2010, *ApJ* in press (arXiv:1002.3619)
- Gebhardt, K., Richstone, D., Ajhar, E. A. et al. 1996, *AJ* 112, 105
- Gebhardt, K., Bender, R., Bower, G., et al. 2000, *ApJ* 539, L13
- Gebhardt, K., Richstone, D., Tremaine, S. et al. 2003, *ApJ* 583, 92
- Ghosh, K. K., Swartz, D.A., Tennant, A. F., Wu, K., Saripalli, L. 2005, *ApJ* 623, 815
- Ghosh, H., Pogge, R. W., Mathur, S., Martini, P., Shields, J. C. 2007, *ApJ* 656, 105
- González-Martín, O., Masegosa, J., Márquez, I., Guainazzi, M., Jiménez-Bailón, E. 2009, *A&A* 506, 1107
- Graham, A.W., et al. 2003, *ApJ* 125, 2951
- Graham, A. W., Guzmán, R. 2003, *AJ* 125, 2936
- Graham, A. W. 2004, *ApJ* 613, L33
- Gualandris, A., Merritt, D. 2008, *ApJ* 678, 780
- Gültekin, K., Richstone, D.O., Gebhardt, K., et al. 2009, *ApJ* 698, 198
- Haardt, F., Maraschi, L. 1993, *ApJ* 413, 507
- Hawley, J. F., Balbus, S. A. 2002, *ApJ* 573, 738
- Ho, L.C., Filippenko, A. V., & Sargent, W.L. W. 1997, *ApJ* 487, 568
- Ho, L. C., Terashima, Y., & Ulvestad, J.S. 2003, *ApJ* 589, 783
- Ho, L.C. 2008, *ARAA* 46, 475
- Ho, L.C. 2009, *ApJ* 699, 626
- Hopkins, P. F., Cox, T. J., Dutta, S. N., Hernquist, L., Kormendy, J., Lauer, T. R. 2009a, *ApJS* 181, 135
- Hopkins, P.F., Murray, N., Thompson, T.A. 2009b, *MNRAS* 398, 303
- Humphrey, P. J., Buote, D. A. 2004, *ApJ* 612, 848
- Jeltema, T.E., Canizares, C.R., Buote, D.A., & Garmire, G.P. 2003, *ApJ* 585, 756
- Jeltema, T. E., Binder, B., Mulchaey, J. S. 2008, *ApJ* 679, 1162
- Jeong, H., Yi, S. K., Bureau, M. et al. 2009, *MNRAS* 398, 2028
- Kaiser, C.R. 2009, *AN* 330, 270
- Kauffmann, G., Heckman, T. M. 2009, *MNRAS* 397, 135
- Kim, D.-W., Fabbiano, G. 2004, *ApJ* 611, 846
- Kim, D.-W., Kim, E., Fabbiano, G., Trinchieri, G. 2008, *ApJ* 688, 931
- Kim, D. W., & Fabbiano, G. 2010, *ApJ* in press (arXiv:1004.2427)
- Körding, E.G., Fender, R.P., Migliari, S. 2006, *MNRAS* 369, 1451
- Kormendy J., Bender R. 1996, *ApJ* 464, L119
- Kormendy, J., Fisher, D.B., Cornell, M.E., Bender, R. 2009, *ApJS* 182, 216
- Kraft, R. P., Vázquez, S. E., Forman, W. R., Jones, C., Murray, S. S., Hardcastle, M. J., Worrall, D. M., Churazov, E. 2003, *ApJ* 592, 129
- Kuntschner, H., Emsellem, E., Bacon, R. et al. 2006, *MNRAS* 369, 497
- Lauer, T. R., Ajhar, E. A., Byun, Y.-I., Dressler, A., Faber, S. M., Grillmair, C., Kormendy, J., Richstone, D., Tremaine, S. 1995, *AJ* 110, 2622
- Lauer T.R., et al. 2007a, *ApJ* 664, 226
- Lauer T.R., et al. 2007b, *ApJ* 662, 808
- Liu, Ji-F., Bregman, J.N. 2005, *ApJS* 157, 59
- Loewenstein, M., Mushotzky, R.F., Angelini, L., Arnaud, K.A., & Quataert, E. 2001, *ApJ* 555, L285
- Magorrian, J., et al. 1998, *AJ* 115, 2285
- Mahadevan, R. 1997, *ApJ* 477, 585
- Malkan, M.A., Gorjian, V., Tam, R. 1998, *ApJS* 117, 25
- Maoz, D. 2007, 377, 1696
- Maraston, C. 2005, *MNRAS* 362, 799
- Mauch, T., Sadler, E. M. 2007, *MNRAS* 375, 931
- McDermid, R. M., Emsellem, E., Shapiro, K. L. et al. 2006, *MNRAS* 373, 906
- Mei, S., Silva, D., Quinn, P. J. 2000, *A&A* 361, 68
- Memola, E., Trinchieri, G., Wolter, A., Focardi, P., Kelm, B. 2009, *A&A* 497, 359
- Merloni, A., Heinz, S. 2007, *MNRAS* 381, 589
- Milosavljevic, M., Merritt, D., Rest, A., van den Bosch, F.C. 2002, *MNRAS* 331, L51
- Mittal, R., Hudson, D. S., Reiprich, T. H., Clarke, T. 2009, *A&A* 501, 835
- Morita, U., Ishisaki, Y., Yamasaki, N., Y., Ota, N., Kawano, N., Fukazawa, Y., Ohashi, T. 2006, *PASJ* 58, 719
- Narayan, R., Yi, I. 1995, *ApJ* 452, 710
- Nagino, R., Matsushita, K. 2009, *A&A* 501, 157
- Nulsen, P., Jones, C., Forman, W., Churazov, E., McNamara, B., David, L., Murray, S. 2009, to appear in the proceedings of "The Monster's Fiery Breath", Eds. Sebastian Heinz & Eric Wilcots (AIP conference series), arXiv:0909.1809
- O’Sullivan, E., Forbes, D.A., Ponman, T.J. 2001, *MNRAS* 328, 461
- O’Sullivan, E., Ponman, T.J. 2004, *MNRAS* 349, 535
- Panessa, F., Barcons, X., Bassani, L., Cappi, M., Carrera, F. J., Ho, L. C., Pellegrini, S. 2007, *A&A* 467, 519
- Parriott, J. R., Bregman, J. N. 2008, *ApJ* 681, 1215

- Pasquali, A., van den Bosch, F.C., Rix, H.-W. 2007, *ApJ* 664, 738
- Pellegrini S., Ciotti L. 1998, *A&A* 333, 433
- Pellegrini, S. 1999, *A&A* 351, 487
- Pellegrini, S., Cappi, M., Bassani, L., Della Ceca, R., Palumbo, G.G.C. 2000, *A&A* 360, 878
- Pellegrini, S., Venturi, T., Comastri, A., Fabbiano, G., Fiore, F., Vignali, C., Morganti, R., Trinchieri, G. 2003b, *ApJ* 585, 677
- Pellegrini, S. 2005a, *MNRAS* 364, 169
- Pellegrini, S. 2005b, *ApJ* 624, 155
- Pellegrini, S., Baldi, A., Kim, D. W., Fabbiano, G., Soria, R., Siemiginowska, A., Elvis, M. 2007a, *ApJ* 667, 731
- Pellegrini, S., Siemiginowska, A., Fabbiano, G., Elvis, M., Greenhill, L., Soria, R., Baldi, A., Kim, D. W. 2007b, *ApJ* 667, 749
- Pian, E., Romano, P., Maoz, D., Cucchiara, A., Pagani, C., La Parola, V. 2009, *MNRAS* 401, 677
- Proga, D., Begelman, M. C. 2003a, *ApJ* 582, 69
- Proga, D., Begelman, M. C. 2003b, *ApJ* 592, 767
- Ptak, A., Yaqoob, T., Mushotzky, R., Serlemitsos, P., Griffiths, R. 1998, *ApJ* 501, L37
- Rampazzo, R., Alexander, P., Carignan, C., et al. 2006, *MNRAS* 368, 851
- Rest, A., van den Bosch, F. C., Jaffe, W., Tran, H., Tsvetanov, Z., Ford, H. C., Davies, J., & Schafer, J. 2001, *AJ* 121, 2431
- Rinn, A. S., Sambruna, R. M., Gliozzi, M. 2005, *ApJ* 621, 167
- Sansom, A. E., O'Sullivan, E., Forbes, D.A., Proctor, R. N., Davis, D. S. 2006, *MNRAS* 370, 1541
- Schawinski, K., et al. 2007, *ApJS* 173, 512
- Schawinski, K., et al. 2010, *ApJ* 711, 284
- Sivakoff, G.R., Sarazin, C.L., & Carlin, J.L. 2004, *ApJ* 617, 262
- Soria, R., Fabbiano, G., Graham, A. W., Baldi, A., Elvis, M., Jerjen, H., Pellegrini, S., Siemiginowska, A. 2006a, *ApJ* 640, 126
- Soria, R., Graham, A. W., Fabbiano, G., Baldi, A., Elvis, M., Jerjen, H., Pellegrini, S., Siemiginowska, A. 2006b, *ApJ* 640, 143
- Terashima, Y., & Wilson, A. S. 2003, *ApJ* 583, 145
- Terlevich, A. I., Forbes, D. A. 2002, *MNRAS* 330, 547
- Thomas, D., Maraston, C., Bender, R., Mendes de Oliveira, C. 2005, *ApJ* 621, 673
- Tonry, J.L., Dressler, A., Blakeslee, J.P., et al. 2001, *ApJ* 546, 681
- Trujillo, I., Erwin, P., Asensio Ramos, A., Graham, A.W. 2004, *AJ* 127, 1917
- Trinchieri, G., Pellegrini, S., Fabbiano, G., et al. 2008, *ApJ*, 688, 1000
- Vasudevan, R.V., Fabian, A.C. 2007, *MNRAS* 381, 1235
- Winter, L.M., Mushotzky, R.F., Reynolds, C.S., Tueller, J. 2009, *ApJ* 690, 1322
- Worrall, D. 2002, *NewAR* 46, 121
- Yamasaki, N. Y., Ohashi, T., Furusho, T. 2002, *ApJ* 578, 833
- Zhang, Z., Xu, H., Wang, Y., An, T., Xu, Y., Wu, X. 2007, *ApJ* 656, 805
- Zhang, W.M., Soria, R., Zhang, S. N., Swartz, D.A., Liu, J.F. 2009, *ApJ* 699, 507